Ab initio simulation of non-Abelian braiding statistics in topological superconductors

Takumi Sanno [1,*] Shunsuke Miyazaki,[1] Takeshi Mizushima,[1,†] and Satoshi Fujimoto[1,2,‡]

[1]*Department of Materials Engineering Science, Osaka University, Toyonaka, Osaka 560-8531, Japan*

[2]*Center for Quantum Information and Quantum Biology, Institute for Open and Transdisciplinary Research Initiatives, Osaka University, Toyonaka, Osaka 560-8531, Japan*

We numerically investigate non-Abelian braiding dynamics of vortices in two-dimensional topological super-conductors, such as *s*-wave superconductors with Rashba spin-orbit coupling. Majorana zero modes (MZMs) hosted by the vortices constitute a topological qubit, which offers a fundamental building block of topological quantum computation. As the MZMs are protected by $\mathbb{Z}_2$ invariant, however, the Majorana qubit and quantum gate operations may be sensitive to intrinsic decoherence caused by MZM hybridization. Numerically simulating the time-dependent Bogoliubov–de Gennes equation without assuming *a priori* existence of MZMs, we examine quantum noises on the unitary operators of non-Abelian braiding dynamics due to interactions with neighboring MZMs and other quasiparticle states. We demonstrate that after the interchange of two vortices, the lowest vortex-bound states accumulate the geometric phase $\pi/2$, and errors stemming from dynamical phases are negligibly small, irrespective of interactions of MZMs. Furthermore, we numerically simulate the braiding dynamics of four vortices in two-dimensional topological superconductors, and discuss an optimal braiding condition for realizing the high performance of non-Abelian statistics and quantum gate operations of Majorana-based qubits.

I. INTRODUCTION

A paramount challenge for realizing quantum computers is physical implementations of fault-tolerant quantum computation because a coupling of a quantum state to environment gives rise to unavoidable decoherence. It has been proposed that a topological phase of matter hosting non-Abelian anyons provides the hardware constitution of fault-tolerant quantum computation [1,2], where topologically protected anyons lead to degenerate ground states unaffected by local perturbations and braiding such anyons implements noise-free quantum gate operations.

A Majorana fermion is a self-Hermitian relativistic particle which is equivalent to its own antiparticle [3]. Such fermion emerges as a special kind of Bogoliubov quasiparticles bound at defects in topological superconductors, such as vortices and edges. The observations of Majorana zero modes (MZMs) have been reported in superfluid ³He [4–6], unconventional superconductors [7,8], superconducting nanowires [9–22], ferromagnetic atomic chains [23], quantum anomalous Hall insulator-superconductor junction [24,25], planar Josephson junctions [26], and so on [27,28]. Recently, Machida *et al.* developed a dilution-refrigerator based STM working below 90 mK, which uncovered the existence of the zero-energy vortex-bound states in the iron-base superconductor Fe(Se,Te) [29]. Similar signals of Majorana bound states have also been observed in Ref. [30]. The MZMs are protected by a topological invariant. The existence of $2n$ MZMs leads to topologically protected ground states which span the 2^{n-1}-dimensional Hilbert space and can be utilized as topological qubits. When MZMs are well isolated from other Bogoliubov quasiparticles, they behave as non-Abelian anyons obeying the non-Abelian statistics, i.e., braiding MZMs can implement quantum gates to manipulate the topological qubit. This is a unique character of MZMs, and topological superconductors with MZMs can provide a platform for realizing topological quantum computation [2,31–39].

MZMs in class-D topological superconductors are, however, protected by $\mathbb{Z}_2$ topological invariant [40,41]. When two neighboring vortices approach, MZM hybridization between neighboring MZMs lifts the degeneracy from zero energy to E_+ and E_-, and a pair of Majorana bound states smoothly connects to topologically trivial vortex-bound states. Thus, a single qubit composed of four MZMs may be sensitive to intrinsic decoherence caused by quasiparticle hybridization [42,43]. The period of braiding operation T may satisfy the characteristic timescale [2]

$$\delta E_{\mathrm{CdGM}}^{-1} \ll T \ll \delta E_{\mathrm{M}}^{-1}. \qquad (1)$$

In this paper, we set $\hbar = 1$. The lower bound $\delta E_{\mathrm{CdGM}}^{-1}$ is to avoid the nonadiabatic transition of MZMs to higher-energy vortex-bound states [44–50], i.e., the Caroli–de Gennes–Matricon (CdGM) states [51], where the typical level spacing of vortex-bound states is $\delta E_{\mathrm{CdGM}} \sim \Delta_0^2/E_{\mathrm{F}}$, where Δ_0 and E_{F} are the bulk superconducting gap and the Fermi energy, respectively (see Fig. 1). The upper bound of the braiding period is associated with the hybridization of neighboring MZMs, which leads to the splitting and oscillation of the

*sanno@blade.mp.es.osaka-u.ac.jp
†mizushima@mp.es.osaka-u.ac.jp
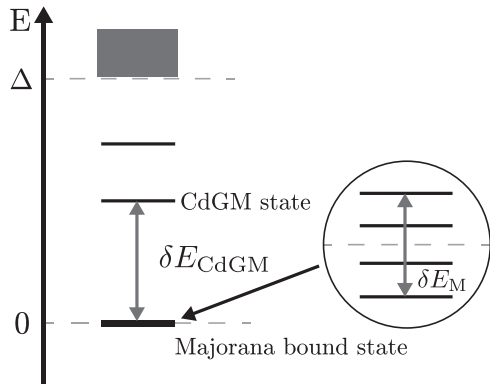‡fuji@mp.es.osaka-u.ac.jp

FIG. 1. Schematic of splitting MZMs embedded in quasiparticle excitation spectrum. The splitting of MZMs and the level spacing from the higher CdGM states are denoted by δE_{M} and δE_{CdGM}, respectively. These determine the lower and upper bounds of the timescale of braiding dynamics: adiabatic condition $T^{-1} \ll \delta E_{\mathrm{CdGM}}$ and nonadiabatic transitions between the energy levels of the hybridized MZMs $T^{-1} \gg \delta E_{\mathrm{M}}$.

ground-state energies as a function of the inter-Majorana distance R as $\delta E_{\mathrm{M}} \equiv E_+ - E_- \propto \cos(k_{\mathrm{F}}R)e^{-R/\xi}$, where the Fermi wavelength k_{F}^{-1} and the superconducting coherence length $\xi = k_{\mathrm{F}}/m\Delta_0$ determine the scale of the oscillation and splitting.

Although numerical simulation of non-Abelian statistics has been demonstrated in one-dimensional superconducting nanowires [52–60], the *ab initio* simulation of non-Abelian braiding dynamics and phase accumulation in two-dimensional class-D superconductors has been lacking. In contrast to nanowire systems, where hybridization between MZMs in different wires is suppressed by gate potentials, MZMs in vortices in two-dimensional systems are not immune to the hybridization effect. MZM hybridization and nonadiabatic dynamics of MZMs may disturb the non-Abelian statistics and give rise to intrinsic decoherence of Majorana qubits. It is indispensable to clarify an optimal braiding protocol for realizing the high performance of non-Abelian braiding dynamics, based on *ab initio* simulations. Understanding the impact of such intrinsic decoherences on Majorana-based qubits is a pressing issue.

In this paper, we present *ab initio* simulation of non-Abelian statistics in two-dimensional topological superconductors, and numerically study intrinsic decoherence caused by quasiparticle hybridization and nonadiabatic braiding dynamics. By numerically simulating the time-dependent Bogoliubov–de Gennes (TDBdG) equation without assuming *a priori* existence of MZMs, we demonstrate the non-Abelian statistics of quantized vortices in two-dimensional trijunction network of s-wave superconductors with Rashba spin-orbit coupling [61–63] and the Fu-Kane model [64]. We note that in addition to class-D topological superconductors, our numerical method is generalizable to other topological classes which may host symmetry-protected multiple MZMs. We first show that the particle-hole symmetry prohibits the direct transition between particle-hole symmetric MZMs. This ensures that after the interchange of two vortices, the ground state

acquires the nontrivial geometric phase $\pi/2$, irrespective of interactions of MZMs. Such transition rule and geometric phase in the braiding dynamics of a two-vortex system are confirmed by numerically solving the TDBdG equation. We succeeded in extracting the geometric phase and dynamical phases from *ab initio* simulations and evaluating quantum noises on the braiding operators, i.e., the unitary operators of quantum gates. Furthermore, we perform numerical simulations of braiding dynamics in a four-vortex system, which constitutes a single topological qubit. The numerical simulations with an optimal braiding period clearly demonstrate that an initially encoded ground state is transferred to another nearly degenerate ground state by interchanging two vortices, i.e., the demonstration of non-Abelian braiding statistics with high accuracy. On the other hand, if the braiding period approaches the upper bound, the dynamical phase stemming from the splitting of ground states causes serious quantum errors of non-Abelian braiding dynamics and quantum gate operations. We discuss the upper and lower bounds of the timescale for realizing the high performance of non-Abelian braiding statistics and quantum gate operations of Majorana-based qubits.

The organization of this paper is as follows. In Sec. II, we describe the theoretical framework and numerical method of the TDBdG equation and discuss the impact of the particle-hole symmetry on nonadiabatic transition between the energy levels of hybridized MZMs. We also present the Hamiltonian relevant to class-D topological superconductors, and present a protocol to implement the braiding dynamics of vortex singularities in superconducting trijunction systems. In Sec. III, we show the numerical results of braiding dynamics in two-vortex systems, and compute the geometric phase that vortex-bound states accumulate after the interchange of vortices. In Sec. IV, we investigate the case of four-vortex systems and present the numerical simulation of braiding dynamics in the trijunction network hosting MZMs. Section V is devoted to conclusions and discussions on disturbance of non-Abelian statistics and decoherence of Majorana-based qubits due to hybridization and nonadiabaticty. The numerical results of braiding dynamics in superconductor-topological insulator heterostructures, i.e., the Fu-Kane model, are presented in the Appendix.

II. TIME-DEPENDENT BOGOLIUBOV–DE GENNES EQUATION

The dynamics of quasiparticles in superconductors is governed by the TDBdG equation. In this section we first summarize the basic properties of MZMs in class-D topological superconductors. Employing the adiabatic approximation and utilizing the Majorana conditions and the particle-hole symmetry, we derive the selection rules for transition between Bogoliubov quasiparticles. We also present trijunction systems formed by s-wave superconductors with Rashba spin-orbit interaction. The numerical results in superconductor-topological insulator heterostructures, i.e., the Fu-Kane model, are shown in the Appendix, where the impact of the chiral symmetry on the braiding dynamics is emphasized.

A. TDBdG equation

We start to introduce the Bogoliubov quasiparticle operator $\eta_n(t)$ as

$$\hat{\eta}_n(t) = \sum_i [u_{n,i}^*(t)\hat{c}_i + v_{n,i}^*(t)\hat{c}_i^\dagger], \qquad (2)$$

where $\hat{c}_i$ and $\hat{c}_i^\dagger$ are the annihilation and creation operators of electrons at a site i. The time evolution of the quasiparticle operator is governed by the wave functions $u_{n,i}(t)$ and $v_{n,i}(t)$. The TDBdG equation to describe the time evolution of quasiparticles is derived from the equation of motion for $\hat{\eta}_n(t)$. We suppose that at $t = 0$, the system is in equilibrium. The corresponding quasiparticle energy E_n and wave functions $|\varphi_{n,i}\rangle \equiv [u_{n,i}, v_{n,i}]^{\text{tr}} = [u_{n,i}(0), v_{n,i}(0)]^{\text{tr}}$ (a^{tr} is the transpose of a matrix a) are obtained from the BdG equation

$$\mathcal{H}_{\text{BdG}}(0)|\varphi_{n,i}\rangle = E_n|\varphi_{n,i}\rangle, \qquad (3)$$

where $i \equiv (i_x, i_y)$ and n denote a site on the two-dimensional square lattice and the label of the quasiparticle energy E_n, respectively. The BdG Hamiltonian is given by

$$[\mathcal{H}_{\text{BdG}}(t)]_{ij} = \begin{pmatrix} \varepsilon_{ij}(t) & \Delta_{ij}(t) \\ \Delta_{ij}^\dagger(t) & -\varepsilon_{ij}^*(t) \end{pmatrix}, \qquad (4)$$

where $\varepsilon(t)$ is the single-particle Hamiltonian density and $\Delta(t)$ is the pair potential. The Hamiltonian of class-D topological superconductors obeys only the particle-hole symmetry,

$$C\mathcal{H}_{\text{BdG}}(t)C^{-1} = -\mathcal{H}_{\text{BdG}}(t), \qquad (5)$$

where C is particle-hole operator with $C^2 = +1$. This implies that the quasiparticle state with a positive energy $E_n > 0$ is accompanied by the negative-energy state with $-E_n$, and the quasiparticle operator obeys

$$\hat{\eta}_{E_n}^\dagger(t) = \hat{\eta}_{-E_n}(t). \qquad (6)$$

The time evolution of the Bogoliubov quasiparticle operators in Eq. (2) is governed by the TDBdG equation for the quasiparticle wave functions

$$i\frac{\partial}{\partial t}|\psi(t)\rangle = \mathcal{H}_{\text{BdG}}(t)|\psi(t)\rangle. \qquad (7)$$

The state vector is defined in the particle-hole space as $|\psi(t)\rangle_i \equiv [u_i(t), v_i(t)]^{\text{tr}}$, where we impose the initial condition $|\psi(t = 0)\rangle = |\varphi_n\rangle$.

B. Majorana fermions in class-D superconductors

Owing to the particle-hole symmetry, the zero-energy quasiparticle is the equal superposition of the particle and hole components with $u_{E=0}^* = v_{E=0}$:

$$\hat{\gamma} \equiv \hat{\eta}_{E=0} = \sum_i u_{E=0,i}^* \hat{c}_i + \text{H.c.}, \qquad (8)$$

which obeys the Majorana condition $\hat{\gamma} = \hat{\gamma}^\dagger$. The zero-energy quasiparticle states appear in quantized vortices of class-D topological superconductor, which are protected by $\mathbb{Z}_2$ topological number [40,41]. This implies that the pairwise zero modes are gapped out by the hybridization of wave functions. Suppose class-D topological superconductors with $2N$ vortices hosting $2N$ MZMs, which are well separated from other

quasiparticle states. The BdG Hamiltonian then reduces to the tight-binding model composed of $2N$ MZMs,

$$\mathcal{H}_{\text{eff}} = i\sum_{\langle i,j\rangle} J_{ij}\hat{\gamma}_i\hat{\gamma}_j, \qquad (9)$$

where the Majorana operators bound at ith vortex $\hat{\gamma}_i$ obey $\{\hat{\gamma}_i, \hat{\gamma}_j\} = \delta_{ij}$. The hopping energy J_{ij} corresponds to the energy splitting of MZMs due to hybridization [42,43]

$$J_{ij} \propto \frac{\cos(k_{\text{F}}R_{ij} + \alpha)}{\sqrt{k_{\text{F}}R_{ij}}}\exp\left(-\frac{R_{ij}}{\xi}\right), \qquad (10)$$

where $2\alpha = \arctan(k_{\text{F}}\xi)$. The rapid oscillation of MZMs in the scale of the Fermi wavelength k_{F}^{-1} represents MZM hybridization and the envelope of J_{ij} is determined by the superconducting coherence length $\xi = k_{\text{F}}/m\Delta_0$ and the distance between γ_i and γ_j, R_{ij}. This hybridization gives rise to finite splitting of ground-state degeneracy.

In this paper, however, we discuss the non-Abelian statistics of Bogoliubov quasiparticles from the direct simulation of Eq. (7). The numerical simulation of the TDBdG equation deals with the dynamics of Bogoliubov quasiparticles, i.e., complex fermions, rather than Majorana fermions $\hat{\gamma}_j(t)$. To demonstrate the non-Abelian braiding dynamics without assuming *a priori* existence of MZMs, we have to obtain the Majorana fermions $\hat{\gamma}_n^1(t)$ and $\hat{\gamma}_n^2(t)$ at the energy eigenstate E_n from the Bogoliubov quasiparticles $\eta_n(t)$, and map the time evolution of $\eta_n(t)$ onto the Majorana braiding dynamics $\hat{\gamma}_n^1(t)$ and $\hat{\gamma}_n^2(t)$. For this purpose, we decompose a spinless complex fermion $\hat{\eta}_n(t)$ associated with the energy eigenstate E_n into a pair of Majorana fermions $\hat{\gamma}_n^1$ and $\hat{\gamma}_n^2$ as

$$\hat{\gamma}_n^1(t) = \frac{1}{\sqrt{2}}[\hat{\eta}_n(t) + \hat{\eta}_n^\dagger(t)], \qquad (11)$$

$$\hat{\gamma}_n^2(t) = -\frac{i}{\sqrt{2}}[\hat{\eta}_n(t) - \hat{\eta}_n^\dagger(t)]. \qquad (12)$$

The Majorana operators obey

$$\{\hat{\gamma}_n^i(t), \hat{\gamma}_m^j(t)\} = \delta_{ij}\delta_{nm} \qquad (13)$$

($i, j = 1, 2$). In general, a system with N complex fermions can be represented by $2N$ Majorana fermions $\{\hat{\gamma}_n^i\}_{n=1,...,N}^{i=1,2}$. The N complex fermions allow one to introduce 2^N-dimensional Fock states

$$|a_1 a_2 \ldots a_N\rangle = \bigotimes_{n=1}^N |a_n\rangle \equiv \bigotimes_{n=1}^N (\hat{\eta}_n^\dagger)^{a_n}|0\rangle, \qquad (14)$$

where $a_n = \{0, 1\}$ is the occupation number of the quasiparticle state with E_n. The eigenvector $|a_n = 0\rangle$ is the vacuum of the Bogoliubov quasiparticle with an eigenenergy E_n and $|1\rangle = \hat{\eta}_n^\dagger|0\rangle$ is the occupied state. The 2^N degenerate ground states are lifted by the tunneling splitting of $2N$ MZMs. We also note that although the BdG Hamiltonian violates the particle-number conservation, the particle-hole symmetry ensures the conservation of the fermion parity. Hence, the Fock state is an eigenvalue of the parity operator $\hat{P} = (-1)^{\hat{F}}$, where $\hat{F} = \sum_{i,\sigma} c_{i,\sigma}^\dagger c_{i,\sigma}$ is the fermion-number operator. The fermion parity conservation splits the Fock space to the 2^{N-1}-dimensional subsectors of the fermion parity. In the limit of

$E_n \to 0$, the Majorana operator $\hat{\gamma}_n^i$ reduces to the MZM $\hat{\gamma}_i$ bound at a vortex core.

Let us consider a system with $2N$ vortices. When the vortices are well isolated from each other, they host N particle-hole symmetric pairs of zero-energy Bogoliubov quasiparticles. The intervortex tunneling of the quasiparticles leads to the dispersive bandlike structure with the bandwidth δE_{M}. The interchange of vortex-bound Bogoliubov quasiparticles can be implemented by braiding vortices with a time period T. As shown in Fig. 1, vortex systems in class-D topological superconductors have two typical energy scales, the level spacing between MZMs and non-Majorana vortex states, $\delta E_{\mathrm{CdGM}} \sim O(\Delta_0^2/\varepsilon_{\mathrm{F}})$, and the splitting of MZMs, $\delta E_{\mathrm{M}} \sim \cos(k_{\mathrm{F}}R)e^{-R/\xi}$. We assume that the "Majorana band" is well separated from higher CdGM states, i.e., $\delta E_{\mathrm{M}} \ll \delta E_{\mathrm{CdGM}}$, and the braiding operation satisfies the adiabatic regime

$$T \gg \delta E_{\mathrm{CdGM}}^{-1}. \tag{15}$$

To capture the braiding dynamics of vortex-bound Bogoliubov quasiparticles, we introduce the Majorana representation of the Bogoliubov quasiparticles in Eqs. (11) and (12), where N Bogoliubov quasiparticle states can be represented by $2N$ Majorana fermions $\hat{\gamma}_n^i(t)$. The TDBdG equation (7) describes the unitary evolution of the Bogoliubov quasiparticles as $\hat{\eta}_n(t) \equiv U(t)\hat{\eta}_n(0)U^{\dagger}(t)$. Within the adiabatic condition in Eq. (15), the braiding dynamics of vortex-bound Bogoliubov quasiparticles can be regarded as the unitary time evolution of the Majorana operators,

$$\hat{\gamma}_n^i(t) \equiv U(t)\hat{\gamma}_n^i(0)U^{\dagger}(t). \tag{16}$$

Following Ref. [65], we introduce the SO($2N$) matrix $\mathbf{V}$ which rotates the $2N$-dimensional Majorana operators as

$$\hat{\gamma}_n^i(T) = \sum_{j,m} \mathbf{V}_{nm}^{ij} \hat{\gamma}_m^j(0), \tag{17}$$

where $\mathbf{V}$ is subject to the conservation of the fermion parity. An explicit expression of $\mathbf{V}$ is obtained from the numerical simulation of the TDBdG equation (7). The braiding matrix $U(T)$ is obtained from the computed matrix $\mathbf{V}$ as

$$U(T) = \exp\left(\frac{1}{4}\sum_{ij} \mathbf{D}_{nm}^{ij} \hat{\gamma}_n^i \hat{\gamma}_m^j\right), \tag{18}$$

where $e^{-\mathbf{D}} = \mathbf{V}$ [65]. In Secs. III and IV, we evaluate quantum noise effects on non-Abelian statistics by computing the SO($2N$) matrix $\mathbf{V}$ from the TDBdG equation in class-D topological superconductors with two and four vortices, respectively.

C. Nonadiabatic transition rules and particle-hole symmetry

We start to derive a generic result that the particle-hole symmetry (PHS) imposes selection rules on the transition between instantaneous eigenstates of $\mathcal{H}_{\mathrm{BdG}}(t)$. We consider a superconducting state with $2N$ vortices, where each vortex hosts a single MZM. We introduce a set of time-dependent parameters $\boldsymbol{R}(t) = (R_1(t), ..., R_N(t))$ as a vector in the parameter space. Let $\boldsymbol{R}_i(t)$ be the position of the ith vortex. The interchange of the ith vortex and the jth vortex is implemented by exchanging $\boldsymbol{R}_i(t)$ and $\boldsymbol{R}_j(t)$ to $\boldsymbol{R}_i(T) = \boldsymbol{R}_j(0)$

and $\boldsymbol{R}_j(T) = \boldsymbol{R}_i(0)$, and the twice operation $\boldsymbol{R}_i(2T) = \boldsymbol{R}_i(0)$ defines a cyclic trajectory in the parameter space. The time dependence of the BdG Hamiltonian is described through the parameters $\boldsymbol{R}(t)$ as $\mathcal{H}_{\mathrm{BdG}}(t) \to \mathcal{H}_{\mathrm{BdG}}(\boldsymbol{R})$. Let $|\varphi_n(\boldsymbol{R})\rangle$ be an instantaneous eigenstate of $\mathcal{H}_{\mathrm{BdG}}(\boldsymbol{R})$:

$$\mathcal{H}_{\mathrm{BdG}}(\boldsymbol{R})|\varphi_n(\boldsymbol{R})\rangle = E_n(\boldsymbol{R})|\varphi_n(\boldsymbol{R})\rangle, \tag{19}$$

where $|\varphi_n(\boldsymbol{R})\rangle$ satisfies the orthonormal condition

$$\langle \varphi_n(\boldsymbol{R})|\varphi_m(\boldsymbol{R})\rangle = \delta_{n,m}. \tag{20}$$

We now expand the time evolution of the nth eigenstate in terms of the set of instantaneous eigenstates $\{|\varphi_m(\boldsymbol{R})\rangle\}$ as

$$|\psi_n(t)\rangle = \sum_m C_m^{(n)}(t) e^{-i\int_0^t E_m(t')dt'} |\varphi_m(\boldsymbol{R})\rangle, \tag{21}$$

where $e^{-i\int_0^t E_n(t')dt'}$ is the dynamical phase and we have introduced $n \in \mathbb{Z}$ as labels of eigenstates. The state vector is assumed to obey the initial condition $|\psi_n(t=0)\rangle = |\varphi_n(\boldsymbol{R}(0))\rangle$, corresponding to

$$C_m^{(n)}(t=0) = \delta_{nm}. \tag{22}$$

Substituting Eq. (21) to Eq. (7), the equation for the coefficient $C_m^{(n)}(t) \in \mathbb{C}$ is given as

$$i\partial_t C_m^{(n)}(t) + \sum_k \Pi_{mk}(t) e^{-i\int_0^t \Delta E_{km}(t')dt'} C_k^{(n)}(t) = 0. \tag{23}$$

The Hermitian matrix $\Pi_{mk}(t) = \Pi_{km}^*(t)$ represents the transition probability between mth and kth instantaneous eigenstates, which is given as

$$\Pi_{nm}(t) \equiv i\langle \varphi_n(\boldsymbol{R})|\partial_t \varphi_m(\boldsymbol{R})\rangle. \tag{24}$$

Under the adiabatic approximation, Π_{nm} reduces to an element of the Berry connection matrix.

We consider the braiding dynamics that the operation period T satisfies the adiabatic approximation in Eq. (15), which implies that the higher CdGM states are outside the ground-state (i.e., Majorana fermions) subspace. Consider a class-D topological superconductor with $2N$ vortices. When the intervortex distance is sufficiently large, tunneling probability of quasiparticles between neighboring vortices is negligible, and each vortex hosts an exactly zero-energy state. In such ideal situation, the braiding rule is governed by the matrix $\mathbf{D}$ and the unitary matrix in Eq. (18) reduces to $U(T) = \exp(\frac{\pi}{4}\hat{\gamma}_i\hat{\gamma}_j)$, implying that the MZMs obey non-Abelian statistics. In finite-size systems, however, quasiparticle tunneling between vortices always leads to a nonzero splitting of zero-energy states $\pm\delta E_{\mathrm{M}}$ as in Eq. (10). The Bogoliubov quasiparticle operator after the interchange operation is given by substituting Eq. (21) into Eq. (2) as

$$\hat{\eta}_n(T) = \sum_{m,k} C_m^{(n)}(T) e^{-i\int_0^T E_m(t)dt} B_{mk}\hat{\eta}_k(0). \tag{25}$$

Here we have introduced the matrix element $B_{mk} \equiv \langle \varphi_m(\boldsymbol{R}(0))|\varphi_k(\boldsymbol{R}(T))\rangle$, which describes the transformation of the quasiparticle basis $\hat{\eta}_n(0)$ to $\sum_m B_{nm}\hat{\eta}_m(0)$ after braiding operation. The expression of matrix $U(T)$ in Eq. (18) can be directly read off from Eq. (25). Cheng *et al.* [65] found that tunneling splitting of zero-energy states gives rise to the nonuniversal contributions of dynamical phase and

non-Abelian Berry phase, and the resulting braiding matrix contains a non-negligible error as

$$U(T) = \exp\left[\left(\frac{\pi}{4} - \frac{\mathcal{E}T}{2}\right)\hat{\gamma}^1\hat{\gamma}^2\right], \quad (26)$$

where $\mathcal{E} \sim |\delta E_M|$. As $\mathcal{E}T/2 = O(1)$ for $T \gtrsim \delta E_M^{-1}$, the noise error induced by tunneling splitting becomes significant when the braiding operation is slow compared to the timescale due to tunneling splitting of MZMs. Such serious error can lead to bit-flip error and parity error [65,66].

Therefore, we consider nonadiabatic transitions between splitting MZMs, where the period T of braiding vortices is much faster than the timescale associated with the splitting of degenerate ground states δE_M, i.e.,

$$T \ll \delta E_M^{-1}. \quad (27)$$

As $R \gg \xi$ and $\Delta_0 \gg \varepsilon_F$ in a realistic situation, the energy scales satisfy $\delta E_{CdGM} \gg \delta E_M$, and the operation period obeys the conditions in Eqs. (15) and (27). We also note that within the condition in Eq. (27), $\Delta E_{nm}T \ll 1$ and the dynamical phase due to splitting of MZMs is negligible, $e^{-i\int^t \Delta E_{nm}(t')dt'} \approx 1$. Thus, Eq. (23) is recast into

$$i\partial_t C_m^{(n)}(t) + \sum_k \Pi_{mk}(t)C_k^{(n)}(t) = 0. \quad (28)$$

As the differential equation for $C_m^{(n)}(t)$ is determined by the Berry connection matrix $\Pi(t)$, we clarify the roles of the symmetry and Majorana condition on the matrix $\Pi(t)$. Let us consider Bogoliubov quasiparticles with the energy $E_n > 0$ and the eigenvector $|\varphi_n(\boldsymbol{R}(t))\rangle$. The particle-hole symmetry in Eq. (5) ensures that the positive-energy eigenstate is always accompanied by a negative-energy eigenstate with $-E_n$ and $|\varphi_{-E_n}\rangle = C|\varphi_{+E_n}\rangle$. The Berry connection matrix $\Pi(t)$ is subject to the particle-hole symmetry in Eq. (5) and the orthonormal condition in Eq. (20). These lead to $\langle \varphi_{-E_n}(\boldsymbol{R})|\partial_t\varphi_{+E_n}(\boldsymbol{R})\rangle = \langle \varphi_{-E_n}(\boldsymbol{R})|\partial_t C\varphi_{-E_n}(\boldsymbol{R})\rangle = \frac{1}{2}\partial_t \langle \varphi_{-E_n}(\boldsymbol{R})|C\varphi_{-E_n}(\boldsymbol{R})\rangle = \partial_t \langle \varphi_{-E_n}(\boldsymbol{R})|\varphi_{+E_n}(\boldsymbol{R})\rangle = 0$. Hence, the symmetry prohibits direct transition between the particle-hole symmetric eigenstates

$$\Pi_{+E_n,-E_n}(t) = \Pi_{-E_n,+E_n}(t) = 0. \quad (29)$$

In the same manner, one reads from Eqs. (5) and (20)

$$\Pi_{\mp E_m,-E_n}(t) = -\Pi_{\pm E_m,+E_n}^*(t). \quad (30)$$

The property of the Berry connection matrix described above indicates that transition between particle-hole symmetric MZMs is forbidden by the particle-hole symmetry. Such particle-hole symmetric transition violates the fermion parity. In Sec. III, we demonstrate that the numerical simulation of braiding dynamics is consistent to the transition rules, and the prohibition of particle-hole symmetric transition ensures the acquisition of the geometric phase $\pi/2$, irrespective of the splitting of MZMs, $\delta E_M \neq 0$.

D. *s*-wave superconductors with Rashba spin-orbit interaction

As a model of class-D topological superconductors, we consider an *s*-wave superconductor with spin-orbit interaction

(SOI) [61–63]. The Hamiltonian is given by

$$\mathcal{H} = \mathcal{H}_K + \mathcal{H}_Z + \mathcal{H}_{SOI} + \mathcal{H}_{SC}. \quad (31)$$

The model is composed of the simple building blocks, such as the hopping term ($\mathcal{H}_K$), the magnetic Zeeman term ($\mathcal{H}_Z$), the Rashba SOI ($\mathcal{H}_{SOI}$), and the *s*-wave pairing term ($\mathcal{H}_{SC}$):

$$\mathcal{H}_K = -t_0 \sum_{\langle \boldsymbol{i},\boldsymbol{j}\rangle,\sigma} \hat{c}_{\boldsymbol{i},\sigma}^\dagger \hat{c}_{\boldsymbol{j},\sigma} - \mu \sum_{\boldsymbol{i},\sigma} \hat{c}_{\boldsymbol{i},\sigma}^\dagger \hat{c}_{\boldsymbol{i},\sigma}, \quad (32)$$

$$\mathcal{H}_Z = -\mu_B H_z \sum_{\boldsymbol{i},\sigma,\sigma'} (\sigma_z)_{\sigma,\sigma'} \hat{c}_{\boldsymbol{i},\sigma}^\dagger \hat{c}_{\boldsymbol{i},\sigma'}, \quad (33)$$

$$\mathcal{H}_{SOI} = -\lambda \sum_{\boldsymbol{i}} [(\hat{c}_{\boldsymbol{i}-\hat{\boldsymbol{x}},\downarrow}^\dagger \hat{c}_{\boldsymbol{i},\uparrow} - \hat{c}_{\boldsymbol{i}+\hat{\boldsymbol{x}},\downarrow}^\dagger \hat{c}_{\boldsymbol{i},\uparrow})$$
$$+ i(\hat{c}_{\boldsymbol{i}-\hat{\boldsymbol{y}},\downarrow}^\dagger \hat{c}_{\boldsymbol{i},\uparrow} - \hat{c}_{\boldsymbol{i}+\hat{\boldsymbol{y}},\downarrow}^\dagger \hat{c}_{\boldsymbol{i},\uparrow}) + \text{H.c.}], \quad (34)$$

$$\mathcal{H}_{SC} = \sum_{\boldsymbol{i}} \Delta_s e^{i\theta_i} \hat{c}_{\boldsymbol{i},\uparrow}^\dagger \hat{c}_{\boldsymbol{i},\downarrow}^\dagger + \text{H.c.} \quad (35)$$

Here, $\hat{c}_{\boldsymbol{i},\sigma}^\dagger$ ($\hat{c}_{\boldsymbol{i},\sigma}$) is a creation (annihilation) operator of electrons with spin $\sigma = (\uparrow,\downarrow)$ at site $\boldsymbol{i} = (i_x, i_y)$. In numerical calculations, we set the parameters as $t_0 = 1.0$, $\mu = -6.2$, $\mu_B H_z = 5.0$, $\lambda = 2.0$, and $\Delta_s = 2.5$ and scaled with t_0. This choice of parameters ensures that odd number of MZMs exist in a vortex core.

E. Numerical method

To demonstrate the braiding dynamics of vortices and non-Abelian statistics, we numerically solve the TDBdG equation (7) for two ($N = 1$) and four ($N = 2$) MZMs in Secs. III and IV, respectively. The time evolution of the quasiparticle state from $|\psi(t)\rangle$ to $|\psi(t + \Delta t)\rangle$ is governed by the time-evolution operator $\hat{U}(t + \Delta t; t)$:

$$|\psi(t + \Delta t)\rangle = \hat{U}(t + \Delta t; t)|\psi(t)\rangle. \quad (36)$$

In general, the time-evolution operator is given by

$$\hat{U}(t + \Delta t; t) = \hat{T}\exp\left[-i\int_t^{t+\Delta t} dt' \mathcal{H}_{BdG}(t')\right], \quad (37)$$

which is approximately reduced to $\hat{U}(t + \Delta t; t) \approx \exp[-i\mathcal{H}(t)\Delta t]$ for small Δt. We expand the time-evolution operator in terms of the Chebyshev polynomials [67]. The similar method is utilized for the simulation of the braiding dynamics in one-dimensional superconducting nanowires [52,55]. We numerically simulate the Majorana braiding dynamics in a two-dimensional network of trijunctions as shown in Fig. 2. This was first proposed by Fu and Kane [64]. Each superconducting island has different U(1) phase, $\phi = 0, \pm 2\pi/3$, and the intersection is regarded as a phase singularity, i.e., a vortex singularity hosting a single MZM. As shown in Fig. 2, the braiding operation of vortices is implemented by changing the U(1) phase ϕ in a superconducting island, which is induced by "quantum" phase slips $\phi \to \phi + 2\pi$. The quantum phase slip has already been observed in a superconducting nanowire [68], and a crossover between quantum and thermal quantum slips has also been realized with changing temperatures [69]. The junction system can be applied as surface code for fault-tolerant quantum computation [70,71].
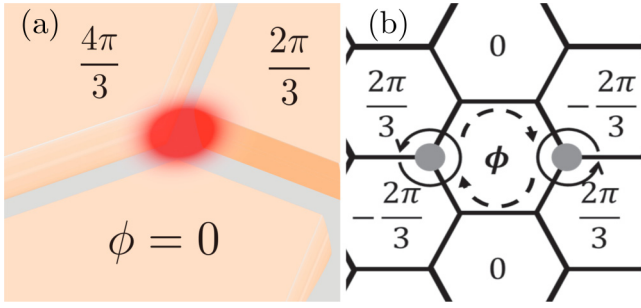
FIG. 2. (a) Schematic of a trijunction hosting a single MZM. Each superconducting island has different phase $\phi = 0, \pm 2\pi/3$ and the intersection is regarded as a phase singularity, i.e., a vortex singularity. (b) Two-dimensional network of trijunctions. The braiding of MZMs is implemented by rotating the U(1) phase ϕ, where the dashed lines indicate the motion of the phase singularities with changing ϕ from 0 to 2π.

III. BRAIDING DYNAMICS IN TWO-VORTEX SYSTEMS

In this section, we consider Majorana braiding dynamics in the Rashba model in Eq. (31) with two vortices, i.e., $N = 1$. When two vortices are well separated and host exactly zero-energy states, the braiding of vortices transforms the Majorana operators $\hat{\gamma}^1$ and $\hat{\gamma}^2$ to $\hat{\gamma}^2$ and $-\hat{\gamma}^1$. The transformation $\hat{\gamma}^j \rightarrow U(T)\hat{\gamma}^j U^{\dagger}(T)$ is compactly represented by the unitary matrix in Eq. (18):

$$U(T) = \exp[\vartheta(T)\hat{\gamma}^1\hat{\gamma}^2], \tag{38}$$

with $\vartheta = \pi/4$. When tunneling splitting of MZMs is not negligible, however, the angle $\vartheta(T)$ is deviated from the ideal value by quantum noises arising from the extra contributions of the dynamical phase and Berry phase as shown in Eq. (26). Here, we will clarify the conditions in which intrinsic noise effects are negligible, and $\vartheta(T)$ approaches $\pi/4$.

Solving the TDBdG equation (7) without assuming *a priori* existence of MZMs, we obtain the information of the transformation of quasiparticles after braiding $\hat{\eta}_n(T) = \sum_m \mathbf{V}_{nm}\hat{\eta}_m(0)$, where $\mathbf{V}_{nm}$ is composed of the transition coefficient $(C_m^{(n)})$, the dynamical phase, and the transformation of the quasiparticle basis (B_{mk}) as in Eq. (25). We compute the transition probability of the initial state $|\psi_n(0)\rangle = |\varphi_n(\boldsymbol{R}(0))\rangle$,

$$P_m^{(n)}(T) \equiv |\langle\varphi_m(\boldsymbol{R}(0))|\psi_n(T)\rangle|, \tag{39}$$

and the accumulation of the geometric phase ϕ_{geo},

$$\phi_{\text{geo}}(T) \equiv \arg\langle\psi_n(0)|\psi_n(T)\rangle - \phi_{\text{dyn}}(T), \tag{40}$$

after the interchange of vortices, where $\phi_{\text{dyn}}(T)$ is the dynamical phase which the wave function accumulates after the interchange of vortices. From $P_m^{(n)}(T)$ and $\phi_{\text{geo}}(T)$, we obtain the explicit expression of the braiding matrix $U(T)$, and extract the effect of nonadiabaticiy and tunneling splitting on quantum noise.

For a class-D superconductor with $2N$ vortices, as shown in Eq. (14), N particle-hole symmetric vortex-bound states η_n construct the 2^N-dimensional Fock space spanned by $|a_1 \ldots a_N\rangle$ $(a_j = \{0, 1\})$. The 2^N degeneracy of the ground states are lifted by the tunneling splitting of $2N$ MZMs. For $N = 1$, the hybridization of two MZMs leads to the energy

splitting $\pm E_+$, where $E_+ = J_{12}$ in Eq. (10). Two Fock states are introduced as the even-parity state $|0\rangle$ and the odd-parity state $|1\rangle \equiv \hat{\eta}_+^{\dagger}|0\rangle$ with $\hat{\eta}_+^{\dagger}$ being the creation operator of the energy eigenstate with $+E_+$. These two states belong to the different parity eigenstate and thus the transition is prohibited unless the particle-hole symmetry is broken.

Here, we would like to mention two fundamental properties of braiding two vortices in class-D topological superconductors. First, the particle-hole symmetry prohibits transition between particle-hole symmetric MZMs. This can be observed by considering the case of two vortices in Eq. (29). Owing to the localized nature of the zero-energy vortex-bound states, the diagonal matrix elements Π_{nn} are exponentially small with respect to R/ξ. In the case of two vortices, the Berry connection matrix results in

$$\Pi_{nm}(t) = 0, \tag{41}$$

i.e., $i\partial_t C_m^{(n)}(t) = \mathbf{0}$. This implies that the fluctuation of the fermion parity $\hat{P}$ is prohibited by the particle-hole symmetry.

Another fundamental property is that when two vortices are braided, the MZM acquires both the geometric phase and dynamical phase. The former represents the transformation of the quasiparticle basis [the B matrix in Eq. (25)]. The latter is attributed to the effect of tunneling splitting of MZMs and results in an extra phase, which may generate a non-negligible error during braiding protocols [65]. According to the braiding rule of strict MZMs, the wave function of the MZM acquires the $\pi/2$ phase shift due to the geometric phase $\langle\psi(0)|\psi(T)\rangle = e^{\pm i\pi/2}$, which is independent of the detail of braiding operation such as period and trajectories of vortices. This can be obtained by introducing a complex fermion composed of two hybridized MZMs $(\hat{\gamma}_+^1, \hat{\gamma}_+^2)$ as $\hat{\eta}_+ = (\hat{\gamma}_+^1 + i\hat{\gamma}_+^2)/2$. A vortex is accompanied by the branch cut which defines the 2π phase jump of the order parameter attaching to the vortex singularity. In exchanging two vortices, the MZM moving across the branch cut experiences the phase shift by π and the Majorana operators are transformed as $\hat{\gamma}_+^1 \rightarrow \hat{\gamma}_+^2$ and $\hat{\gamma}_+^2 \rightarrow -\hat{\gamma}_+^1$. The complex fermion then changes from $\hat{\eta}_+(0) = (\hat{\gamma}_+^1 + i\hat{\gamma}_+^2)/\sqrt{2}$ to $\hat{\eta}_+(T) = e^{-i\pi/2}\hat{\eta}_+(0)$, which is accompanied by the extra phase factor $e^{-i\pi/2}$. Hence, the accumulation of the U(1) phase after braiding operation

$$|\phi_{\text{geo}}(T)| = \pi/2 \tag{42}$$

serves as a direct signature that the braiding dynamics is governed by Eq. (38) with $\vartheta = \pi/4$. The deviation of the accumulated quasiparticle phase from Eq. (42) implies that $\vartheta(T)$ in the braiding matrix is deviated from $\pi/4$, and the accumulation of extra phases due to the adiabaticity and quasiparticle tunneling gives rise to intrinsic errors in the non-Abelian statistics.

To evaluate the geometric phase ϕ_{geo} and the braiding matrix in Eq. (38), we perform the numerical simulation of the TDBdG equation (7). We also compute Eq. (19) to obtain the instantaneous eigenstates at t. We impose the open boundary conditions at the edges of the two-dimensional lattice. Figures 3(a) and 3(b) show the two-dimensional network of the trijunctions, where Φ denotes the phase of the superconducting order parameter. As shown in Fig. 3(c), the braiding operation can be implemented by linearly changing Φ in the
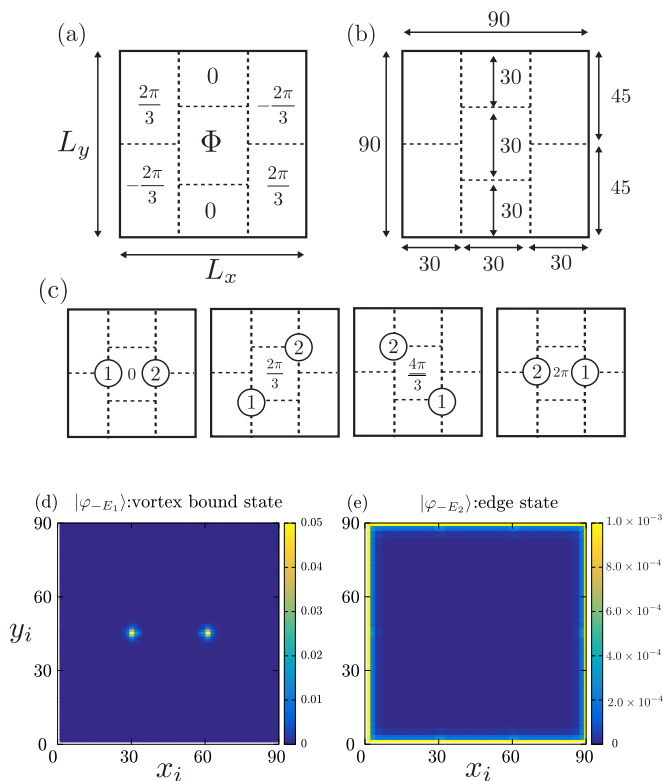
FIG. 3. (a) Schematics of the U(1) phase configuration of the superconducting order parameter for two-vortex simulation. (b) Domain size of calculated systems. (c) Motion of vortex singularities with changing Φ. (d), (e) Spatial profiles of quasiparticle wave functions $\sum_\sigma [|u_{i,\sigma}|^2 + |v_{i,\sigma}|^2]$, in the $|\varphi_{-E_1}\rangle$ and $|\varphi_{-E_2}\rangle$ states when $\Phi = 0$. The former (latter) is identified as the vortex (edge) bound state.
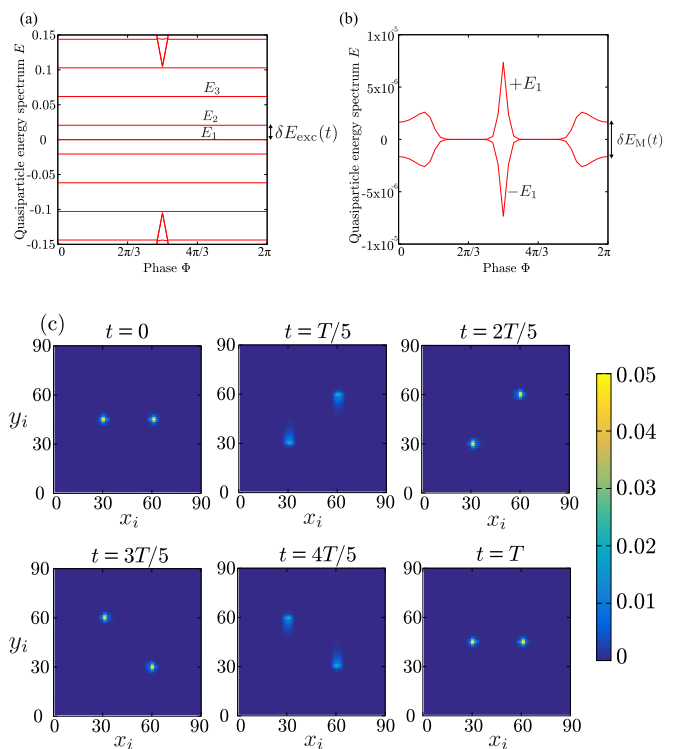

FIG. 4. (a) Evolution of the instantaneous eigenenergies with respect to the phase change of the center domain $\Phi(t)$. (b) Instantaneous eigenenergies of splitting MZMs, where the maximum splitting occurs at $\Phi = \pi$. (c) Time evolution of the quasiparticle wave functions $\sum_\sigma [|u_{i,\sigma}(t)|^2 + |v_{i,\sigma}(t)|^2]$, obtained by solving the TDBdG equation (7). This can be seen in the Supplemental Material [72].

central island from 0 to 2π, as

$$\Phi(t) = 2\pi t/T. \tag{43}$$

We first prepare the initial state $|\psi_n(t = 0)\rangle$ by diagonalizing $\mathcal{H}_{BdG}$ in Eq. (19) with the order-parameter configuration in Fig. 3(a) with $\Phi(t = 0) = 0$. Figures 3(d) and 3(e) show the wave functions of the lowest ($E_1/t_0 = 1.643 \times 10^{-6}$) and second lowest eigenstates ($E_2/t_0 = 2.061 \times 10^{-2}$), which are tightly bound at the vortex and edge, respectively. Numerically solving the TDBdG equation (7) with the given initial state $|\psi_n(t = 0)\rangle$, we simulate the braiding dynamics of two vortices. The spatial profiles of the quasiparticle wave functions during braiding operation, $\sum_\sigma |u_{i,\sigma}(t)|^2 + |v_{i,\sigma}(t)|^2$, are displayed in Fig. 4(c), where $|\psi(t)\rangle = [u_{i,\uparrow}(t), u_{i,\downarrow}(t), v_{i,\uparrow}(t), v_{i,\downarrow}(t)]^T$. The two pronounced peaks follow the time evolution of the vortex singularities generated by the evolution of $\Phi(t)$. At $t = T$, the positions of two peaks return to the original positions of vortex singularities, while we will show below that the wave functions acquire an extra phase, and cannot return to the original form. In Fig. 4(a), we plot the low-lying quasiparticle spectrum of the instantaneous $\mathcal{H}_{BdG}[\boldsymbol{R}(t)]$ as a function of t. The vortex-bound states stay around the zero energy in the whole t, and the nonzero energy states correspond to the edge bound states. We note that the edges are well spatially separated from the vortex

singularities, and the hybridization is negligible during the braiding dynamics. Figure 4(b) shows the enlarged spectrum within $|E| < 3.0 \times 10^{-6}$ corresponding to the splitting energies $+E_+$ and $-E_+$ induced by quasiparticle tunneling between two vortex singularities.

In the numerical simulation, we take the period T of the braiding protocol to satisfy the adiabatic process in Eq. (15) and the nonadiabatic process in (27) within the splitting MZMs. Thus, the braiding period T must satisfy the condition

$$\max[\delta E_M(t)] \lesssim 1/T \lesssim \min[\delta E_{exc}(t)], \tag{44}$$

where $\delta E_M(t)$ is the scales of the splitting energies of MZMs, and $\delta E_{exc}(t)$ is the energy difference between the lowest-energy (splitting MZM) state and lowest non-Majorana state (the higher CdGM state or edge state). The upper and lower bounds of the braiding period are determined from the instantaneous quasiparticle spectrum. As seen in Fig. 4(a), the energy difference between the Majorana band and excited states is almost constant on t. As the splitting of MZMs has the maximum value when $\Phi = \pi$, the upper bound of T is set to the maximum splitting energy. Therefore, the condition of T is given by $50 \lesssim T \lesssim 6.1 \times 10^5$, and T in the numerical simulation is set to $T = 1500 t_0^{-1}$, where $dt = 0.003 t_0^{-1}$. We set $|\varphi_{-E_1}(\boldsymbol{R}(0))\rangle$ as the initial state at $t = 0$. The numerical result of the interchange of two vortices shows that the
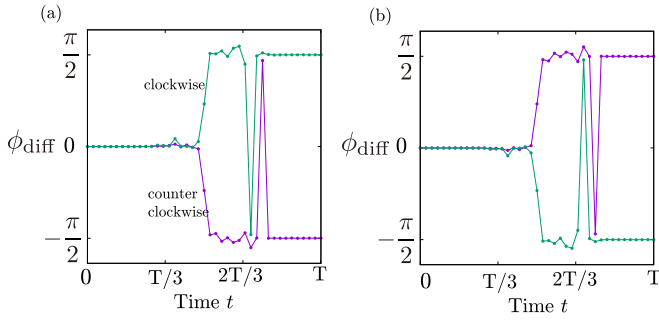
FIG. 5. Time evolution of the phase difference $\psi_{\text{diff}}(t)$ in the $|\varphi_{-E_1}\rangle$ state (a) and the $|\varphi_{+E_1}\rangle$ state (b) in the clockwise (green) and counterclockwise (purple) interchange operation of two vortices.

transition probability from the initial $(-E_1)$ state to the particle-hole symmetric $(+E_1)$ states is found to be

$$P_+^{(-)} = |\langle\varphi_{+E_1}|\psi(T)\rangle|^2 = O(10^{-16}t_0^{-1}), \qquad (45)$$

$$P_-^{(-)} = |\langle\varphi_{-E_1}|\psi(T)\rangle|^2 = 0.997. \qquad (46)$$

This result is consistent with the transition rule in Eq. (29), where the direct transition between splitting MZMs in $N = 1$ is protected by the particle-hole symmetry.

We now extract the dynamical and geometric phases from the numerical simulation of braiding vortices. The accumulation of the phase in braiding dynamics is given as

$$\phi_{\text{diff}}(t) = \arctan\left\{\frac{\text{Im}\,\langle\psi(0)|\psi(t)\rangle}{\text{Re}\,\langle\psi(0)|\psi(t)\rangle}\right\}. \qquad (47)$$

Figures 5(a) and 5(b) show the time evolution of the phase difference $\phi_{\text{diff}}(t)$ in $|\varphi_{-E_1}\rangle$ and $|\varphi_{+E_1}\rangle$, respectively. Here, we plot $\phi_{\text{diff}}(t)$ for the counterclockwise (purple) and clockwise (green) rotation of vortices, which can be implemented by changing the phase $\Phi(0) = 0 \rightarrow \Phi(T) = 2\pi$ and $\Phi(0) = 0 \rightarrow \Phi(T) = -2\pi$ in Fig. 3(a), respectively. We find that after interchange operation the vortex-bound states accumulate the phase $|\phi_{\text{diff}}(T)| = 1.572 \approx \pi/2$, which contains the contributions of both the geometric phase and the dynamical phase. From the energy spectrum and braiding period $T = 1500t_0^{-1}$, the contribution of the dynamic phase factor to $\phi_{\text{diff}}(T)$ is estimated as $O(10^{-3})$. As T increases, the braiding dynamics approaches the adiabatic regime $T \gg \delta E_{\text{M}}^{-1}$, and the noise effect $\phi_{\text{diff}}(T) - \pi/2$ is induced by the dynamical phase. In Fig. 5, it is seen that $\phi_{\text{diff}}(t)$ abruptly jumps around $t = 3T/2$. This is attributed to the peculiarity of the trijunction model in Fig. 3(a), where the signs of vorticities of both vortex singularities after the period are inverted from those in the initial state. However, it turns out that the sign flip of vorticity does not affect the phase accumulation of vortex-bound states.

The counterclockwise motion of vortices is the time-reversal symmetric operation of the clockwise one. The quasiparticles along the two trajectories acquire geometric phase with opposite sign while accumulating the same dynamical phase. To extract the geometric phase from ϕ_{diff}, therefore, we decompose $\phi_{\text{diff}}^{\text{clock}}(T)$ and $\phi_{\text{diff}}^{\text{count}}(T)$ accumulated by the clockwise and counterclockwise interchange
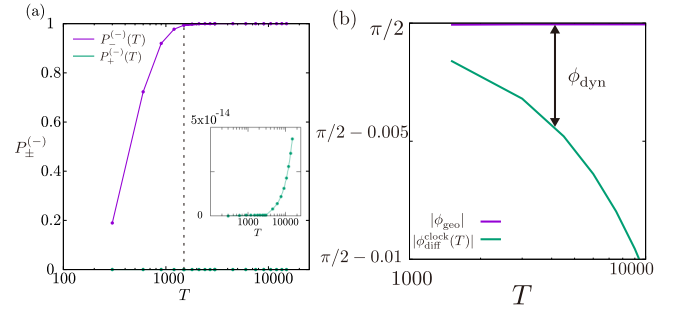

FIG. 6. Transition probabilities $P_\pm^{(-)}$ (a) and the geometric phase ϕ_{geo} (b) as a function of the period of the braiding operation T. In Sec. III, we have discussed the numerical simulation of braiding vortices with $T = 1500t_0^{-1}$ which is denoted by the dashed line in (a).

as

$$\phi_{\text{diff}}^{\text{clock}}(T) = \phi_{\text{geo}} + \phi_{\text{dyn}}, \qquad (48)$$

$$\phi_{\text{diff}}^{\text{count}}(T) = -\phi_{\text{geo}} + \phi_{\text{dyn}}. \qquad (49)$$

The numerical simulation of braiding two vortices shows that the accumulated geometric phase coincides with the expected value $\pi/2$ within numerical accuracy,

$$\phi_{\text{geo}} = [\phi_{\text{diff}}^{\text{clock}}(T) - \phi_{\text{diff}}^{\text{count}}(T)]/2 = -1.570\,79. \qquad (50)$$

Hence, the deviation of the accumulated phase from $\pi/2$ is attributed to the dynamical phase stemming from the hybridization of MZMs.

After the interchange of two vortices, the lowest vortex-bound quasiparticle state accumulates the geometric phase $\phi_{\text{geo}} \approx \pi/2$ and the dynamical phase $\hat{\eta}_+(T) = ie^{i\delta\phi}\hat{\eta}_+(0)$. The deviation of the accumulated phase $\delta\phi \equiv \phi_{\text{diff}}(T) - \pi/2 \approx \phi_{\text{dyn}}$ is attributed to the dynamical phase due to the interaction of MZMs. The interchange of vortices generates the transformation of the Majorana operators $\hat{\gamma}_+^1(t) \equiv [\hat{\eta}_+(t) + \hat{\eta}_+^\dagger(t)]/\sqrt{2}$ and $\hat{\gamma}_+^2(t) \equiv -i[\hat{\eta}_+(t) - \hat{\eta}_+^\dagger(t)]/\sqrt{2}$ as

$$\hat{\gamma}_+^1(T) = -\cos(\delta\phi)\hat{\gamma}_+^2(0) - \sin(\delta\phi)\hat{\gamma}_+^1(0), \qquad (51)$$

$$\hat{\gamma}_+^2(T) = \cos(\delta\phi)\hat{\gamma}_+^1(0) - \sin(\delta\phi)\hat{\gamma}_+^2(0). \qquad (52)$$

This braiding dynamics of quasiparticles is represented by the braiding matrix $U(T)$ in Eq. (38) with

$$\vartheta(T) = \frac{\pi}{4} - \delta\phi. \qquad (53)$$

Hence, $\delta\phi$ is a possible source of quantum disturbance of non-Abelian braiding dynamics.

In Fig. 6, we compute the transition probability $P_\pm^{(-)}$ and the noise of the accumulated phase $\delta\phi$ as a function of the braiding period T. We find that the transition probabilities are $P_-^{(-)} \approx 1$ and $P_+^{(-)} \approx 0$, and the the noise of the accumulated phase is negligible $\delta\phi \ll 1$, when the braiding period satisfies $1000t_0^{-1} \lesssim T\,10\,000t_0^{-1}$. For $T \lesssim 1000t_0^{-1}$, however, $P_-^{(-)}$ significantly decreases with increasing the speed of the braiding operation. The depletion of the norm $P_-^{(-)} \equiv |\langle\varphi_{-E_1}|\psi(t)\rangle|^2$ is attributed to the nonadiabatic transition to the higher CdGM states. These results numerically demonstrate that when the braiding operation satisfies the conditions in Eqs. (15) and

(27), the noise effect due to the interaction of neighboring MZMs is negligible, and the non-Abelian braiding dynamics can be successfully accomplished as in Eq. (38) with $\vartheta(T) \approx \pi/4$. We also note that for $T \gtrsim 10\,000 t_0^{-1}$, the transition probability between the particle-hole symmetric states $P_+^{(-)} \equiv |\langle \varphi_{+E_1}(0)|\psi(t)\rangle|^2$ exponentially increases with respect to T. This corresponds to the adiabatic regime that the braiding period is slower than the timescale of the energy splitting of MZMs, $T \gg \delta E_M^{-1} \sim O(10^5 t_0^{-1})$. As the adiabatic regime is approached, the braiding dynamics of quasiparticles significantly accumulates the dynamical phase, which gives rise to serious errors in the braiding matrix $U(T)$ from $\vartheta(T) = \pi/4$.

IV. BRAIDING DYNAMICS IN FOUR-VORTEX SYSTEMS

In this section, we consider the braiding dynamics of systems with four vortices. Let us first consider an ideal situation that vortices are well separated from each other, and each vortex hosts a single MZM. Let $\hat{\gamma}^i$ be the Majorana operator bound at the ith vortex ($i = 1, 2, 3, 4$), and $\hat{c}_{12} = (\hat{\gamma}^1 + i\hat{\gamma}^2)/\sqrt{2}$ and $\hat{c}_{34} = (\hat{\gamma}^3 + i\hat{\gamma}^4)/\sqrt{2}$ be the operators of complex fermions. The two-dimensional Fock space is spanned by the degenerate ground states $|00\rangle$ and $|11\rangle = \hat{c}_{12}^\dagger \hat{c}_{34}^\dagger |00\rangle$, which defines a single qubit. The manipulation of the qubit can be implemented by the interchange of ith and jth vortices U_{ij}, which is defined in Eqs. (18) and (38). The operation $U_{12}(T)$ leads to the $\pi/4$ phase rotation of the qubit, while the operations $U_{13}(T)$ and $U_{13}(2T) = [U_{13}(T)]^2$ implement the Hadamard gate $|00\rangle \to (|00\rangle + |11\rangle)/\sqrt{2}$ and the NOT gate $|00\rangle \to |11\rangle$, respectively.

Here, we examine the noise effect on non-Abelian statistics of vortices and quantum gates by numerically simulating the TDBdG equation with four vortices. In this section we present the numerical simulation in the junctions of s-wave superconductors with the Rashba SOI. The braiding dynamics in the Fu-Kane model, which is the heterostructure of a topological insulator and an s-wave superconductor, is shown in the Appendix. As the zero-energy vortex-bound states in class-D topological superconductors are protected by a $\mathbb{Z}_2$ invariant, and the quasiparticle tunneling between neighboring vortices during braiding operation causes the non-negligible splitting of the ground states. To address the effect of quasiparticle hybridization, we consider the four-vortex system shown in Fig. 7(a), which is composed of a two-dimensional array of the superconducting domains with different U(1) phases. To exclude the contribution of edge states, we impose the periodic boundary condition. The size of the unit cell is $L_x \times L_y$ and the periodic boundary conditions along the x and y directions are imposed as

$$\hat{\Delta}(i_x = L_x, i_y) = \hat{\Delta}(i_x = 1, i_y = i_y + L_y/2), \quad (54)$$

$$\hat{\Delta}(i_x, i_y = L_y) = \hat{\Delta}(i_x, i_y = 1), \quad (55)$$

respectively. Below we mainly show the numerical results for $L_x = 52$ and $L_y = 104$ [see Fig. 7(b)]. As shown in Fig. 7(c), the phase configuration at $\Phi = 0$ hosts the four vortex singularities labeled by "1," "2," "3," and "4." Without loss of generality, we take the condition $D_{12}, D_{34} < D_{13}, D_{24}$, where 1-2 and 3-4 vortices are tightly paired. In the numerical calculation, we set $D_{12} = D_{34} = 20$ and $D_{13} = D_{24} = 32$,
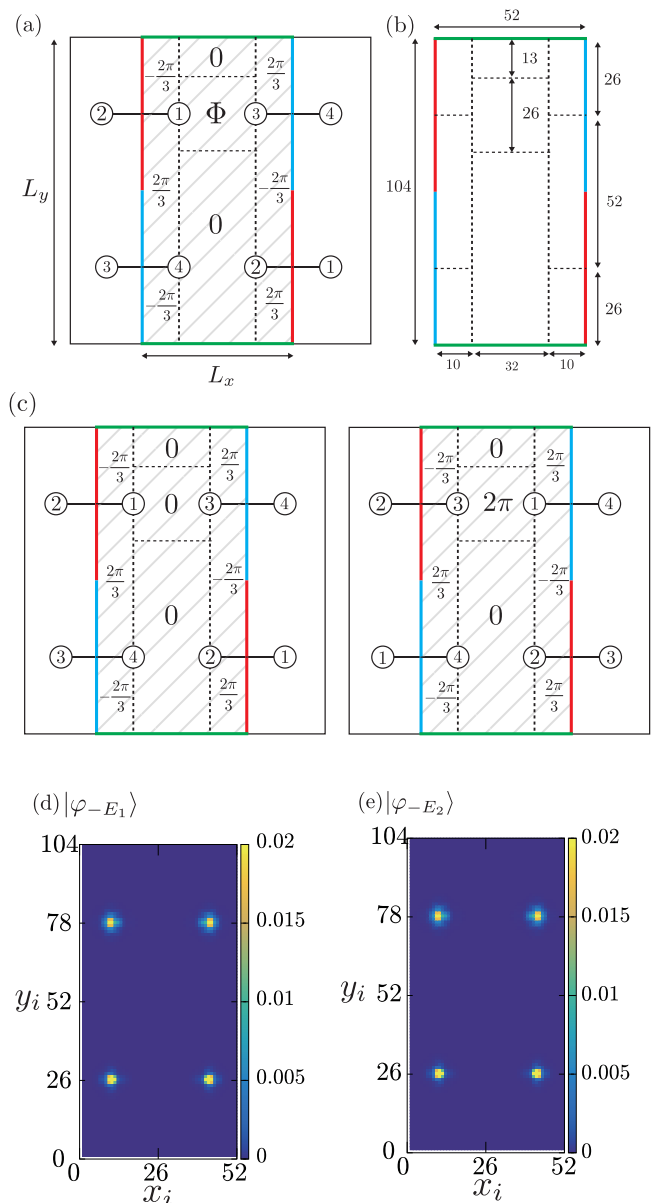

FIG. 7. (a), (b) Configuration of four vortices made from superconducting junctions for numerical simulation of braiding dynamics. The lines with same color are identified by the periodic boundary conditions in Eqs. (54) and (55). The dashed region is the unit cell of trijunction network and its numerical setup in (b) satisfies the condition $D_{12}, D_{34} < D_{13}, D_{24}$. (c) The advance of Φ in a superconducting domain interchanges vortex singularities labeled by "1" and "3." (d), (e) Spatial profiles of the quasiparticle wave functions with the energy $-E_1$ and $-E_2$, $\sum_\sigma [|u_{i,\sigma}|^2 + |v_{i,\sigma}|^2]$, where the U(1) phase is set to be $\Phi = -2\pi$.

where D_{12} and D_{34} (D_{13} and D_{24}) are the intrapair (interpair) distance. Without loss of generality, we take the condition $D_{14}, D_{23} < D_{13}, D_{24}$. The set of other parameters is same as that in Sec. III. The rotation of the superconducting phase Φ interchanges the interpair vortex singularities labeled by "1" and "3" in a counterclockwise direction. We start with $\Phi = -2\pi$ and evolve Φ to 2π to implement the twice interchange of "1" and "3" vortex singularities.
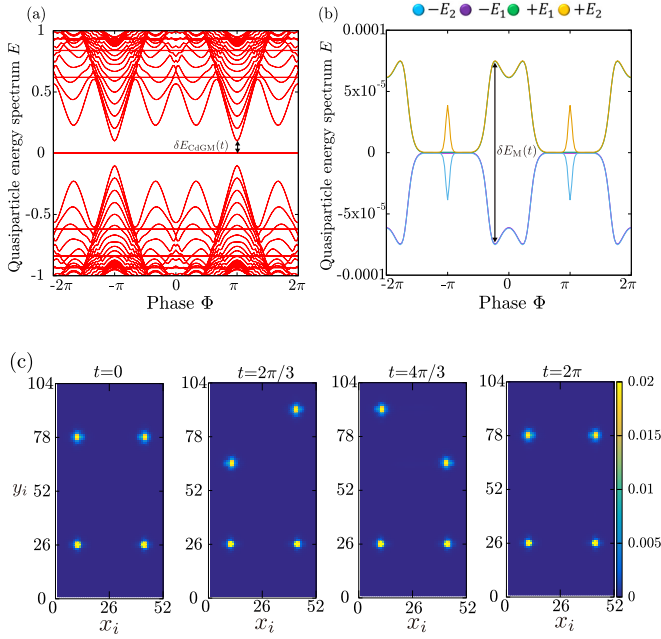
FIG. 8. (a) Evolution of the instantaneous eigenenergies with respect to the U(1) phase Φ. The lower bound of the braiding period T is determined by the inverse of the minimum splitting between MZMs and the higher CdGM states around $\Phi = \pm\pi$, $\delta E_{\mathrm{CdGM}}^{-1}(t)$. (b) Instantaneous eigenenergies of splitting MZMs (Majorana band), where the inverse of the maximum splitting occurs around $\Phi = \pm\pi/150$, $\delta E_{\mathrm{M}}^{-1}(t)$, determines the upper bound of T. (c) Time evolution of the quasiparticle wave functions $\sum_{\sigma}[|u_{i,\sigma}(t)|^2 + |v_{i,\sigma}(t)|^2]$ is obtained by solving the TDBdG equation (7). This can be seen in the Supplemental Material [72].

When the intervortex distance is macroscopically large, the ground states are doubly degenerate and the braiding of inter-pair vortices can manipulate the degenerate ground states. In numerical calculation, however, the finite-size effect gives rise to the quasiparticle tunneling between neighboring vortices and the hybridization of MZMs hosted by each vortex. The splitting energy levels of four MZMs are referred to as $\pm E_1$ and $\pm E_2$, where $E_1 < E_2$. Figures 7(d) and 7(e) show the quasiparticle wave functions of the lowest ($E_1/t_0 = 6.118 \times 10^{-5}$) and second lowest ($E_2/t_0 = 6.155 \times 10^{-5}$), which are tightly bound at vortex singularities. Figure 8(a) also shows the instantaneous eigenenergies of the BdG Hamiltonian with varying Φ from -2π to 2π. When $\Phi = \pm\pi$, the energy-level spacing between the Majorana band and higher CdGM states, $\delta E_{\mathrm{CdGM}}(t)$, has the minimum value, which defines the lower bound of the braiding period T. Figure 8(b) shows the quasiparticle energy spectrum around zero energy, i.e., the Majorana band. The energy width of the Majorana band $\delta E_{\mathrm{M}}(t)$ becomes maximum at $\Phi = \pm\pi/150$. This determines the upper bound of T. Hence, the condition of the braiding period T is evaluated as $1.77t_0^{-1} < T < 2.7 \times 10^6 t_0^{-1}$. In numerical simulation of the TDBdG equation (7), we take the braiding period as $T = 1440 t_0^{-1}$ and $dt = 0.003 t_0^{-1}$.

We now present the numerical simulation of the braiding dynamics of $\hat{\eta}_{E_{-1}}^{\dagger} \hat{\eta}_{E_{-2}}$. We compute the TDBdG equation (7), with the initial conditions $|\psi(t=0)\rangle = |\varphi_{E_{-1}}\rangle$ and $|\psi(t=0)\rangle = |\varphi_{E_{-2}}\rangle$. The U(1) phase is evolved from $\Phi(t =$
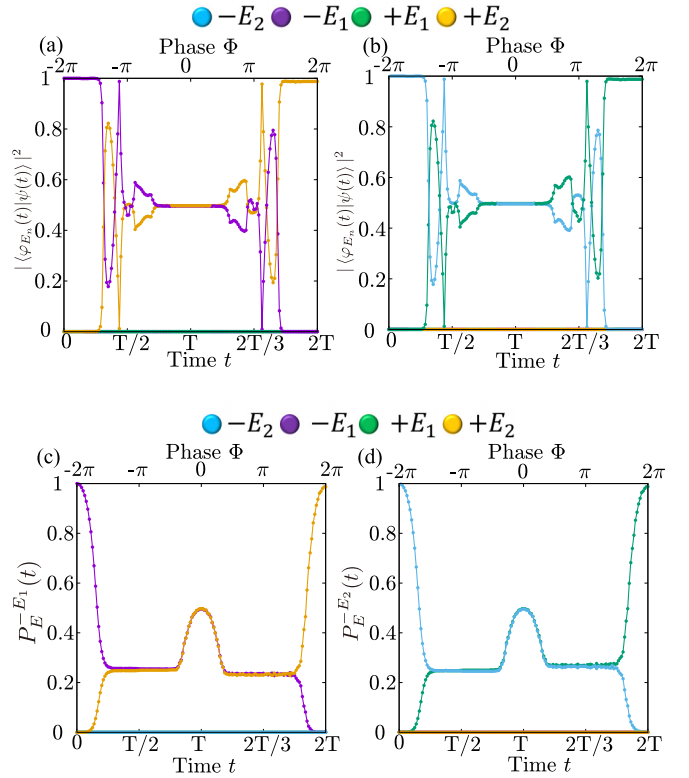

FIG. 9. (a), (b) Projections of $|\psi(t)\rangle$ onto the instantaneous eigenstates $|\varphi_{E_n}(\Phi(t))\rangle$, where the initial states in (a) and (b) are $|\varphi_{-E_1}(\Phi(0))\rangle$ and $|\varphi_{-E_2}(\Phi(0))\rangle$, respectively. (c), (d) Projection of $|\psi(t)\rangle$ onto the encoded state $|\varphi_{-E_1}(\Phi(0))\rangle$ (c) and $|\varphi_{-E_2}(\Phi(0))\rangle$ (d). The twice interchange of vortices ($t = 2T$) causes the transition of the quasiparticle states with $-E_1$ and $-E_2$ to the eigenstates with $+E_2$ and $+E_1$, respectively. This transition implies the unitary transformation of the encoded state $|00\rangle$ to $|11\rangle \equiv \hat{\eta}_{E_1}^{\dagger} \hat{\eta}_{E_2}^{\dagger} |00\rangle$.

$0) = -2\pi$ to $\Phi(t = 2T) = 2\pi$ linearly on time, $\Phi(t) = -2\pi + 2\pi t/T$. Figure 8(c) shows the time evolution of the quasiparticle wave functions from $t = 0$ to T. The peaks of the quasiparticle wave functions trace the motion of vortex singularities driven by the U(1) phase rotation. The numerical results thus demonstrate that the interchange of vortices can be implemented by the rotation of the U(1) phase Φ.

To unveil the quasiparticle dynamics during the braiding of vortices, we compute the projection of the time evolution of the encoded (initial) state $|\varphi_{E_n}(\Phi(0))\rangle$ onto the instantaneous eigenstates. Figures 9(a) and 9(b) show the projections of $|\psi(t)\rangle$ onto the instantaneous eigenstates $|\varphi_{E_n}(\Phi(t))\rangle$, $|\langle \varphi_{E_n}(\Phi(t))|\psi_{E_m}(t)\rangle|^2$, where the initial states in (a) and (b) are $|\varphi_{-E_1}(\Phi(0))\rangle$ and $|\varphi_{-E_2}(\Phi(0))\rangle$, respectively. The quasiparticle during the braiding operation is composed of the instantaneous eigenstates with $-E_1$ and $+E_2$ ($-E_2$ and $+E_1$). The direct transition to the particle-hole symmetric eigenstate $+E_1$ ($+E_2$) is never observed, and the eigenstate with the energy $+E_1$ ($+E_2$) does not contribute to the dynamics of $-E_1$ ($-E_2$). This observation is understandable from the differential equation with the Berry connection matrix

$$i\partial_t \boldsymbol{C}(t) = \hat{B}(t)\boldsymbol{C}(t), \qquad (56)$$

where $\boldsymbol{C}(t)$ is $(C_{+E_1}, C_{-E_1}, C_{+E_2}, C_{-E_2})$ and $\hat{B}(t)$ is

$$\hat{B}(t) \equiv \begin{pmatrix} \hat{0}_{2\times2} & \hat{A}_{E_2,E_1} \\ \hat{A}^\dagger_{E_2,E_1} & \hat{0}_{2\times2} \end{pmatrix}.$$

As mentioned in Sec. II C, Eq. (41) indicates that direct transition between pairs is suppressed by PHS, which can be confirmed by projecting the evolution state $|\psi(t)\rangle$ to instantaneous eigenstates.

As an important consequence, it can be seen from Figs. 9(a) and 9(b) that the transition from $-E_1$ ($-E_2$) to $+E_2$ ($+E_1$) achieves $|\langle\varphi_{+E_2}(\Phi(t))|\psi_{-E_1}(t)\rangle|^2 = |\langle\varphi_{-E_1}(\Phi(t))|\psi_{-E_1}(t)\rangle|^2 = 0.5$ $[|\langle\varphi_{+E_1}(\Phi(t))|\psi_{-E_2}(t)\rangle|^2 = |\langle\varphi_{-E_2}(\Phi(t))|\psi_{-E_2}(t)\rangle|^2 = 0.5]$ at $t \sim 3T/4$ before the interchange operation of vortices completes at $t = T$. Around $t \sim T/4$, the interchanging vortex moves across the branch cut associated with another interchanging vortex. It is also seen from Figs. 9(a) and 9(b) that the transition probabilities $|\langle\varphi_{+E_2}(\Phi(t))|\psi_{-E_1}(t)\rangle|^2$ and $|\langle\varphi_{+E_1}(\Phi(t))|\psi_{-E_2}(t)\rangle|^2$ tend to be saturated to 1 before $t = 2T$. These results indicate that the Hadamard and NOT gates may be accomplished with small error even if the interchanged vortices do not precisely return to the initial positions.

We also compute the transition probability of the encoded (initial) state $|\psi_m(t=0)\rangle = |\varphi_m(\Phi(t))\rangle$ to the initial state

$$P_n^{(m)}(t) \equiv |\langle\varphi_n(\Phi(0))|\psi_m(t)\rangle|^2, \quad (57)$$

which is the projection of $|\psi(t)\rangle$ onto the encoded state. Figures 9(c) and 9(d) show the projection of $|\psi_m(t)\rangle$ onto the quasiparticle states $|\varphi_n(\Phi(0))\rangle$ at $t = 0$, $P_n^{(m)}(t)$. The interchange of vortices at $t = T$ leads to the equal superposition of the encoded $-E_1$ ($-E_2$) state with the $+E_2$ ($+E_1$) state. Another interchange operation completely transforms the encoded $-E_1$ ($-E_2$) state to the $+E_2$ ($+E_1$) state. The braiding dynamics of "1" and "3" vortices generates the transformation of Bogoliubov quasiparticles as $\hat{\eta}_{+E_1} \to (\hat{\eta}_{+E_1} + e^{i\alpha}\hat{\eta}^\dagger_{+E_2})/\sqrt{2}$ and $\hat{\eta}_{+E_2} \to (\hat{\eta}_{+E_2} + e^{i\alpha}\hat{\eta}^\dagger_{+E_1})/\sqrt{2}$. Hence, the twice interchange operation of the vortices transforms

$$\hat{\eta}_{+E_1}\hat{\eta}_{+E_2} \to \hat{\eta}^\dagger_{+E_1}\hat{\eta}^\dagger_{+E_2}, \quad (58)$$

which implies that braiding vortices generate the unitary evolution of the encoded state $|00\rangle \to |11\rangle$.

In Fig. 10, we compute the transition probabilities $P_E^{-E_1}$ as the function of the twice braiding period $2T$. Twice braiding of MZMs shows the transition from initial state to another degenerate states. We find that the transition probabilities $P_{+E_2}^{-E_1} \approx 1$, $P_{-E_1}^{-E_1} \approx 0$, when the twice braiding period $2T$ satisfies $1000t_0^{-1} \lesssim 2T \lesssim 10\,000t_0^{-1}$. For $2T \lesssim 1000t_0^{-1}$, $P_{+E_2}^{-E_1}$ remarkably decreases with increasing the speed of the braiding operation. This is caused by the nonadiabatic transition to the higher vortex-bound states. For $2T > 10\,000t_0^{-1}$, $P_{+E_1}^{-E_1}$ is gradually decreasing, while $P_{-E_1}^{-E_1}$ is gradually increasing. This implies that the braiding dynamics approaches the adiabatic limit, where the twice braiding period $2T$ is slower than the timescale of the energy splitting of MZMs. Thus, in the adiabatic limit $T \to \infty$, the braiding dynamics does not show non-Abelian statistics due to the effect of MZM hybridization.

The condition of the braiding operation period T is $1.77t_0^{-1} \lesssim T \lesssim 2.7 \times 10^6 t_0^{-1}$. If one takes spin-orbit coupling constant as $\lambda = 50$ meV, the condition leads to 55.7 fs $\lesssim T \lesssim$
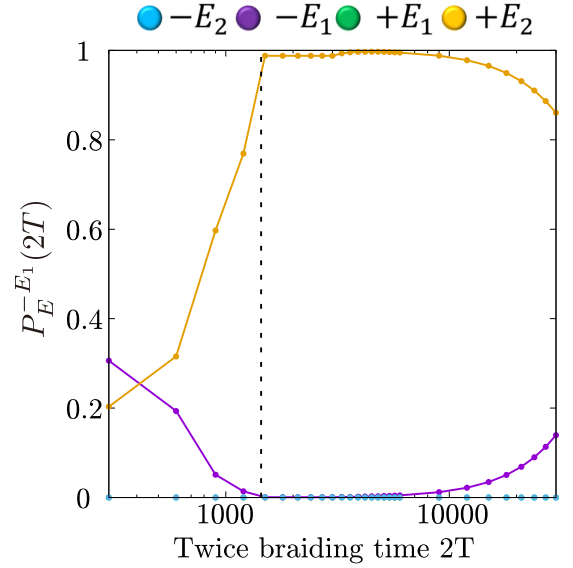

FIG. 10. Transition probabilities $P_E^{-E_1}$ as the function of the period of the twice braiding operation $2T$. The solid lines with different colors correspond to the projection onto the eigenstates with $E = \pm E_2$ and $\pm E_1$, where the color is same as that in Fig. 9. The dashed line denotes $T = 1440t_0^{-1}$ which is the braiding period taken in Figs. 8 and 9.

85.1 ns. The lower bound represents the condition to avoid the nonadiabatic transition to the higher CdGM states, which is determined by the level spacing between CdGM states $\delta E_{CdGM} \sim \Delta_0^2/E_F$. As an example, we take the values of the superconducting gap and the Fermi energy in Fe(Se,Te) as $\Delta_0 = 1.5$ meV [73] and $E_F \sim 10$ meV [74], which leads to the level spacing $\Delta_0^2/E_F \sim 0.23$ meV. With these energy scales, the lower bound in Eq. (1) is estimated as the order of $\delta E_{CdGM}^{-1} \sim 10$ ps. In contrast, the upper bound exponentially increases as a function of the ratio of the intervortex distance and the superconducting coherence length, and depends on an applied magnetic field. For the intervortex distance 100 nm and the vortex core radius 10 nm at $B = 1$ T in Ref. [29], the upper bound is estimated as the order of 0.48 s. These two bounds are well separated and different by several orders of magnitude with realistic material parameters.

V. CONCLUDING REMARKS

In conclusion, we have demonstrated non-Abelian statistics of vortices in two-dimensional class-D topological superconductors. An s-wave superconductor with Rashba spin-orbit coupling, which we mainly consider here, is known as a prototype of class-D topological superconductors hosting MZMs. However, such zero-energy states are protected by a $\mathbb{Z}_2$ invariant and fragile against the hybridization due to the overlap of the wave functions. In this work, we have numerically solved the TDBdG equation which incorporates the effect of the quasiparticle tunneling between neighboring vortices. This calculation does not assume *a priori* existence of MZMs. In addition to s-wave superconductors with the Rashba spin-orbit coupling, we have also presented the numerical simulation of non-Abelian braiding statistics in the

heterostructure of an s-wave superconductor and a topological insulator in the Appendix.

In Sec. III, we have demonstrated that the interchange of two vortices can be implemented by rotating the U(1) phase in trijunction systems and extracted the geometric phase from the numerical simulation of braiding dynamics. Owing to the suppression of direct transition between particle-hole symmetric eigenstates, the vortex-bound quasiparticles accumulate the nontrivial geometric phase $\pi/2$ in the interchange of two vortices. We have presented the upper and lower bounds of the braiding timescale, within appropriate period the non-Abelian braiding statistics obeys $U(T)$ in Eq. (38) with $\vartheta = \pi/4$, irrespective of MZM hybridization.

In Sec. IV, we have also performed the numerical simulation of braiding dynamics in topological superconductors with four vortices. It has been demonstrated that the quasiparticle dynamics hosted by vortex singularities obey the non-Abelian statistics. The numerical simulation shows that the twice interchange operation of two vortices gives rise the the transition of quasiparticle operators $\hat{\eta}_{+E_1}^{\dagger}\hat{\eta}_{+E_2} \rightarrow \hat{\eta}_{+E_1}^{\dagger}\hat{\eta}_{+E_2}^{\dagger}$, which is the nature of non-Abelian statistics: $|00\rangle \rightarrow |11\rangle$. From the numerical simulation, we have evaluated the adiabatic and nonadiabatic errors due to the energy splitting of MZMs and interactions to the higher-energy CdGM states. The braiding timescale is determined by the energy gap between MZMs and CdGM and the energy splitting of MZMs. We find that the twice interchanging operation of the two vortices does not show non-Abelian statistics in the region where the braiding period T is close to the upper limit. This leads to the serious error when the implementation of quantum gate using Majorana-based qubits.

We would like to point out some issues on the configuration of superconducting junctions for realizing braiding dynamics in experiments. The U(1) phase Φ in the superconducting island (see Figs. 3 and 7) may be controlled by changing an external voltage or phase slip [68]. In s-wave superconductors, however, Josephson current due to the phase difference between islands flows across domain walls, which may make such junction thermodynamically unstable. Here, we would like to mention that Majorana fermions exist in a vortex core of a d-wave superconductor with an antisymmetric spin-orbit interaction and a nonzero magnetic field [75], which is protected by a topological invariant in spite of the presence of bulk gapless nodal quasiparticles. In high-T_c superconductors, it has been reported that integer and half-integer Josephson vortices are trapped in grain boundaries and tricrystal points [76–78]. Although a d-wave superconductor offers a potential platform for realizing non-Abelian braiding statistics, the contribution of gapless nodal quasiparticles may significantly disturb the braiding dynamics of MZMs. In addition to superconducting heterostructures, the iron-based superconductor Fe(Se,Te) is a prime candidate of bulk topological superconductors hosting Majorana bound states in vortices [29,30]. Motion of vortices hosting MZMs might be manipulated by using a spin-polarized STM tip [79] or magnetic force microscopy [80]. Another important issue, which has not been discussed here, is the decoherence of the Majorana qubit due to interaction with thermal environment [81,82], where the fermion occupation in the Majorana qubit may leak into the thermal bath. How nodal quasiparticles and thermal excitations disturb non-Abelian braiding dynamics remains issues for future research.

Lastly, we would like to mention that the numerical method presented here is generalizable to the other systems, including superconducting nanowires, planar Josephson junctions, and the other topological classes with symmetry-protected MZMs [83–85]. In particular, the topological superconducting phase in proximitized semiconductor nanowires provides more promising platform for topological quantum computation. However, the braiding dynamics in the T junction network of nanowires may suffer intrinsic and extrinsic disturbances. This includes a nonuniformity of the proximitized superconducting gap introducing geometric dependence to the dynamical phase, thermally excited quasiparticles, the fluctuation of fermion parity to the ancilla nanowires, and gate voltage fluctuations. If a system maintains an antiunitary symmetry $\mathcal{T}^2 = -1$, processing quantum information with Majorana Kramers pairs is sensitive to local perturbations that cause local mixing of degenerate ground states via time-dependent symmetry-preserving coupling to bulk quasiparticles [86,87]. All these may be harmful for the coherence of Majorana qubits and quantum gates. The *ab initio* simulation on such decoherence remains as future works. In addition, another fundamental question arises. How does the particle-number conservation affect the braiding dynamics and the performance of topological quantum computation with Majorana zero modes? In accordance with the number-conserving theory [88,89], the dynamics of Bogoliubov quasiparticles is inevitably accompanied by the dynamics of Cooper pairs. This is also a fundamental and important issue to be addressed in the future.

APPENDIX: NON-ABELIAN STATISTICS IN THE FU-KANE MODEL

In this Appendix, we demonstrate non-Abelian statistics in the Fu-Kane model [64]. The model comprises a topological insulator with an s-wave superconductor layer, yielding a proximitized two-dimensional Dirac fermion. This can be a prototypical system of a topological superconductor hosting MZMs.

Here we start with the effective Hamiltonian of the Fu-Kane model $\mathcal{H}_{FK}$ [90,91], which is written in the momentum

space as

$$\mathcal{H}_{\text{FK}} = \begin{pmatrix} g_{\boldsymbol{k}} - \mu & M_{\boldsymbol{k}} & \Delta_{\boldsymbol{k}} & 0 \\ M_{\boldsymbol{k}} & -g_{\boldsymbol{k}} - m\sigma_z & 0 & 0 \\ \Delta_{\boldsymbol{k}}^* & 0 & -g_{-\boldsymbol{k}}^{\text{tr}} + \mu & -M_{\boldsymbol{k}} \\ 0 & 0 & -M_{\boldsymbol{k}} & g_{-\boldsymbol{k}}^{\text{tr}} + m\sigma_z \end{pmatrix},$$

$$\text{(A1)}$$

where

$$g_{\boldsymbol{k}} = 2\lambda(\sigma_y \sin k_x - \sigma_x \sin k_y), \quad \text{(A2)}$$

$$M_{\boldsymbol{k}} = 2\tau(2 - \cos k_x - \cos k_y), \quad \text{(A3)}$$

$$\delta_{\boldsymbol{k}} = i\sigma_y \Delta_0. \quad \text{(A4)}$$

The Hamiltonian acts on an eight-component Nambu spinor $(c_{\uparrow,1,\boldsymbol{k}}^\dagger, c_{\downarrow,1,\boldsymbol{k}}^\dagger, c_{\uparrow,2,\boldsymbol{k}}^\dagger, c_{\downarrow,2,\boldsymbol{k}}^\dagger, c_{\downarrow,1,-\boldsymbol{k}}, -c_{\uparrow,1,-\boldsymbol{k}}, c_{\downarrow,2,-\boldsymbol{k}}, -c_{\uparrow,2,-\boldsymbol{k}})$, where $c_{\sigma,i,\boldsymbol{k}}^\dagger$ is a creation operator of a fermion with spin $\sigma = \uparrow, \downarrow$ and momentum $\boldsymbol{k}$ on the surface $i = 1, 2$ of the topological insulator. The diagonal blocks describe the gapless surface Dirac fermions on the two surfaces of the topological insulator, and $M_{\boldsymbol{k}}$ generates an energy gap in all the Dirac nodes except those at $\boldsymbol{k} = (0, 0)$. An s-wave superconductivity is induced in one of the surfaces, the surface "1," by proximity effect. To study vortex dynamics, we transform the effective Hamiltonian in the momentum space to a two-dimensional square lattice in the real space. The Hamiltonian in Eq. (A1) includes an exchange interaction on the surface "2," $m\sigma_z$, which induces a gap in the surface states. The term is necessary to remove unwanted gapless excitations from the surface "2" [91].

At $\mu = 0$, the Fu-Kane model maintains the chiral symmetry with γ^5, and the MZMs have a well-defined chirality. The symmetry prohibits the hybridization of MZMs with same chirality, and rigidly protects MZMs with $\mathbb{Z}$ topological invariant rather than $\mathbb{Z}_2$ [92]. The index theorem [93,94] also ensures that N singly quantized vortices host N MZMs, and the chiral symmetry prevents MZMs from hybridization. The deviation from $\mu = 0$ breaks the chiral symmetry, and gives rise to the hybridization. The MZMs bound at vortices start to form a band structure.

Here, we discuss braiding dynamics in the Fu-Kane model with four vortex singularities, where the configuration of four vortices is same as superconducting junctions in Fig. 7. For the numerical simulation, we set the parameter $\tau = 0.9$, $\mu = 4.8$, $\lambda = 2.0$, $m = 0.5$, and $\Delta_0 = 1.6$. We consider a system with four vortices, which hosts two particle-hole symmetric vortex-bound states $\pm E_1$ and $\pm E_2$ as a consequence of the hybridization of four MZMs. Figures 11(a) and 11(b) show the wave function of the lowest ($E_1/\tau = 9.616 \times 10^{-7}$) and second lowest ($E_2/\tau = 9.678 \times 10^{-7}$), $\sum_\sigma [|u_{i,\sigma}(t)|^2 + |v_{i,\sigma}(t)|^2]$.

For numerical simulation of braiding vortices, we start with the initial state $|\varphi_{-E_1}\rangle$. The braiding period is determined in the same manner as that in the main text, i.e., the appropriate period must obey $1.40 \times 10\tau^{-1} \lesssim T \lesssim 2.94 \times 10^5\tau^{-1}$. The lower bound is set to prevent MZMs from nonadiabatic coupling to other quasiparticle states with higher energies, while the upper bound is necessarily to protect non-Abelian braiding dynamics from errors due to dynamical phase accumulation. Numerical simulation demonstrates non-Abelian braiding
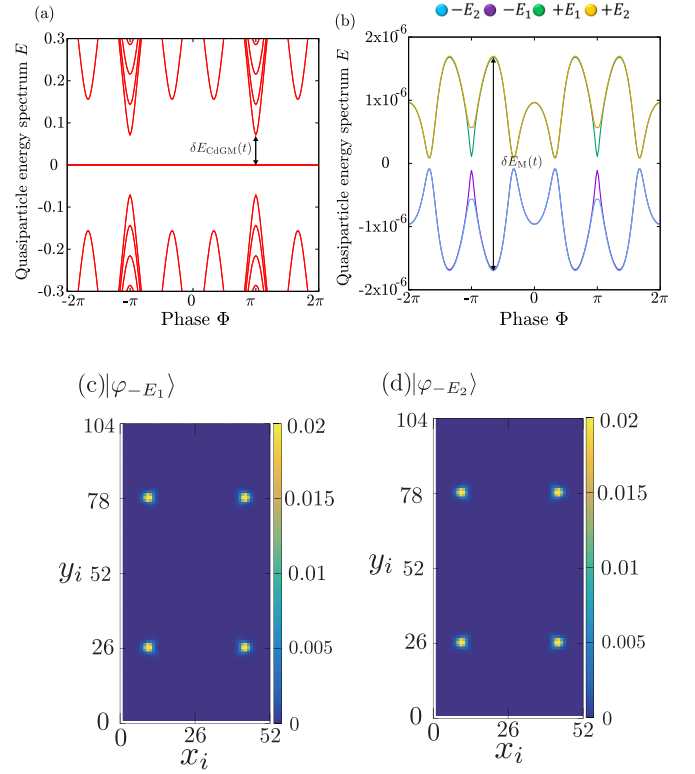

FIG. 11. (a) The lower bound of the braiding period T is determined by the inverse of the minimum splitting between MZMs and the higher CdGM states around $\Phi = \pm\pi$, $\delta E_{\text{CdGM}}^{-1}(t)$. (b) Instantaneous eigenenergies of Majorana band, where the inverse of the maximum splitting occurs around $\Phi = \pm 16\pi/25$, $\delta E_{\text{M}}^{-1}(t)$, determines the upper bound of T. (c), (d) Spatial profiles of the quasiparticle wave function with the energy $-E_1$ and $-E_2$, $\sum_\sigma [|u_{i,\sigma}|^2 + |v_{i,\sigma}|^2]$, where the U(1) phase is set to be $\Phi = -2\pi$.

dynamics with high accuracy as long as the braiding operation satisfies the condition.

In Fig. 12(a), we plot the projection of the time-evolved eigenvector $|\psi(t)\rangle$ onto the instantaneous eigenstates and
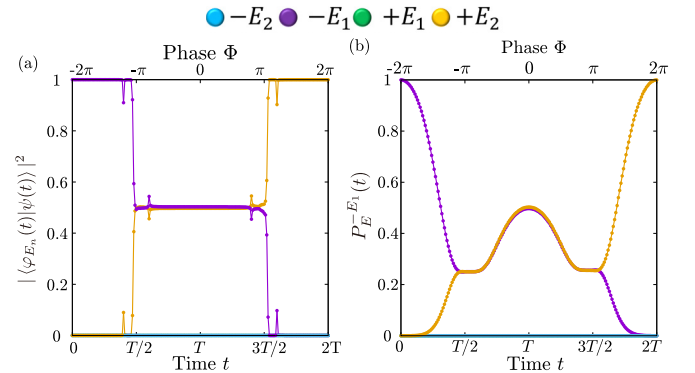

FIG. 12. Projection of $|\psi(t)\rangle$ onto the instantaneous eigenstates (a) and the encoded state $|\varphi_{-E_1}(\Phi(0))\rangle$ (b). where the period T is fixed to $T = 7500\tau^{-1}$. The twice interchange operation of two vortices generates the transition of the quasiparticle states with $-E_1$ to the eigenstate with $+E_2$.
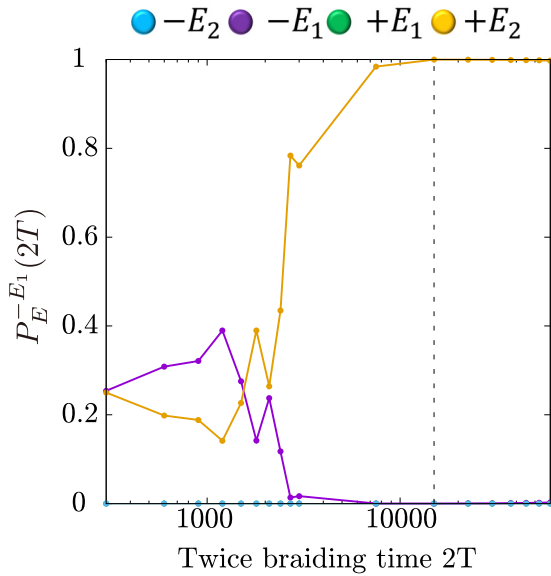
FIG. 13. Transition probabilities $P_E^{-E_1}$ as the function of the period of the twice braiding operation $2T$. The numerical simulation with $T = 7500t_0^{-1}$, which is shown in Fig. 12, is denoted by dashed line.

the encoded state $|\varphi_{-E_1}(\Phi(0))\rangle$ [Fig. 12(b)]. Figure 12(b) also shows the projection of $|\psi(t)\rangle$ onto the encoded state $|\varphi_{-E_1}(\Phi(0))\rangle$, revealing the transition from initial state to another degenerate ground state: $P_E^{-E_1}(T)$. Similarly with the numerical simulation in the Rashba model, both figures demonstrate that the interchange of two vortices in four vortices gives rise to the transition from $-E_1$ to $+E_2$. The time-evolved eigenvector is composed of equal contributions

of the $-E_1$ and $+E_2$ instantaneous eigenstates around $t = T/2$. This implies that one of the interchanging vortices moves across the branch cut around $t = T/2$ and experiences the abrupt 2π-phase rotation.

In Fig. 13, we compute the transition probabilities $P_E^{-E_1}$ as the function of the twice braiding period $2T$. Similarly with Fig. 10, $P_{+E_2}^{-E_1}$ remarkably decreases for $2T \lesssim 10\,000\tau^{-1}$. This deviation is attributed to the nonadiabatic transition from MZMs to the higher-energy quasiparticle states, i.e., nonadiabatic interaction to environment induces the decoherence of the Majorana-based qubit. $P_{-E_1}^{-E_1}$ is not gradually decreasing in Fig. 13. Our numerical results in the Fu-Kane model do not show the deviation of $P_{+E_2}^{-E_1}$ in the adiabatic limit $T \gg \delta E_M^{-1} \sim 10^5$. The numerical simulation with the much slower braiding operation $T \gg 10^5$ is required to realize the adiabatic errors of non-Abelian braiding statistics in the Fu-Kane model.

Let us discuss the timescale of the braiding dynamics in iron-based superconductors Fe(Se,Te). The superconducting gap Δ of Fe(Se, Te) is observed as $\Delta \approx 1.5$ meV [73] and its Fermi energy E_F is $E_F \approx 10$ meV [74]. By using these values, the typical energy spacing between the CdGM states is estimated as $\delta E_{CdGM} \approx \Delta^2/E_F = 0.23$ meV. The level spacing determines the lower bound of the braiding period T. In contrast, the upper bound exponentially increases as a function of the ratio of the intervortex distance and the superconducting coherence length, and depends on an applied magnetic field. For the intervortex distance 100 nm and the vortex core radius 10 nm at $B = 1$ T in Ref. [29], MZM hybridization can be approximated as $\delta E_M \sim \Delta \exp(-R/\xi)/R^{1/2}$ since topological surface states of Fe(Se, Te) are observed around the Γ point [95]. As shown in Fig. 11(a), the minimum gap from MZMs in instantaneous energy spectrum is $\min[\delta E_{CdGM}(t)] = 6.56 \times 10^{-2}$ meV. The condition of the braiding period T is given by 10 ps $\lesssim T \lesssim 0.48$ s. The braiding timescale might be feasible.

[1] A. Kitaev, Anyons in an exactly solved model and beyond, Ann. Phys. **321**, 2 (2006).

[2] C. Nayak, S. H. Simon, A. Stern, M. Freedman, and S. Das Sarma, Non-Abelian anyons and topological quantum computation, Rev. Mod. Phys. **80**, 1083 (2008).

[3] E. Majorana, Teoria simmetrica dell'elettrone e del positrone, Nuovo Cimento **14**, 171 (1937).

[4] S. Murakawa, Y. Tamura, Y. Wada, M. Wasai, M. Saitoh, Y. Aoki, R. Nomura, Y. Okuda, Y. Nagato, M. Yamamoto, S. Higashitani, and K. Nagai, New Anomaly in the Transverse Acoustic Impedance of Superfluid ^{3}He-B with a Wall Coated by Several Layers of ^{4}He, Phys. Rev. Lett. **103**, 155301 (2009).

[5] S. Murakawa, Y. Wada, Y. Tamura, M. Wasai, M. Saitoh, Y. Aoki, R. Nomura, Y. Okuda, Y. Nagato, M. Yamamoto, S. Higashitani, and K. Nagai, Surface Majorana Cone of the Superfluid ^{3}He B Phase, J. Phys. Soc. Jpn. **80**, 013602 (2011).

[6] T. Mizushima, Y. Tsutsumi, T. Kawakami, M. Sato, M. Ichioka, and K. Machida, Symmetry-Protected Topological Superfluids and Superconductors–From the Basics to ^{3}He–, J. Phys. Soc. Jpn. **85**, 022001 (2016).

[7] L. Jiao, S. Howard, S. Ran, Z. Wang, J. O. Rodriguez, M. Sigrist, Z. Wang, N. P. Butch, and V. Madhavan, Chiral superconductivity in heavy-fermion metal UTe$_2$, Nature (London) **579**, 523 (2020).

[8] S. Ran, C. Eckberg, Q.-P. Ding, Y. Furukawa, T. Metz, S. R. Saha, I.-L. Liu, M. Zic, H. Kim, J. Paglione, and N. P. Butch, Nearly ferromagnetic spin-triplet superconductivity, Science **365**, 684 (2019).

[9] V. Mourik, K. Zuo, S. M. Frolov, S. R. Plissard, E. P. A. M. Bakkers, and L. P. Kouwenhoven, Signatures of Majorana fermions in hybrid superconductor-semiconductor nanowire devices, Science **336**, 1003 (2012).

[10] A. Das, Y. Ronen, Y. Most, Y. Oreg, M. Heiblum, and H. Shtrikman, Zero-bias peaks and splitting in an Al-InAs nanowire topological superconductor as a signature of Majorana fermions, Nat. Phys. **8**, 887 (2012).

[11] L. P. Rokhinson, X. Liu, and J. K. Furdyna, The fractional a.c. Josephson effect in a semiconductor-superconductor nanowire as a signature of Majorana particles, Nat. Phys. **8**, 795 (2012).

[12] A. D. K. Finck, D. J. Van Harlingen, P. K. Mohseni, K. Jung, and X. Li, Anomalous Modulation of a Zero-Bias Peak in a

Hybrid Nanowire-Superconductor Device, Phys. Rev. Lett. **110**, 126406 (2013).

[13] H. O. H. Churchill, V. Fatemi, K. Grove-Rasmussen, M. T. Deng, P. Caroff, H. Q. Xu, and C. M. Marcus, Superconductor-nanowire devices from tunneling to the multichannel regime: Zero-bias oscillations and magnetoconductance crossover, Phys. Rev. B **87**, 241401(R) (2013).

[14] M. T. Deng, S. Vaitiekenas, E. B. Hansen, J. Danon, M. Leijnse, K. Flensberg, J. Nygård, P. Krogstrup, and C. M. Marcus, Majorana bound state in a coupled quantum-dot hybrid-nanowire system, Science **354**, 1557 (2016).

[15] S. M. Albrecht, A. P. Higginbotham, M. Madsen, F. Kuemmeth, T. S. Jespersen, J. Nygård, P. Krogstrup, and C. M. Marcus, Exponential protection of zero modes in Majorana islands, Nature (London) **531**, 206 (2016).

[16] H. J. Suominen, M. Kjaergaard, A. R. Hamilton, J. Shabani, C. J. Palmstrøm, C. M. Marcus, and F. Nichele, Zero-Energy Modes from Coalescing Andreev States in a Two-Dimensional Semiconductor-Superconductor Hybrid Platform, Phys. Rev. Lett. **119**, 176805 (2017).

[17] F. Nichele, A. C. C. Drachmann, A. M. Whiticar, E. C. T. O'Farrell, H. J. Suominen, A. Fornieri, T. Wang, G. C. Gardner, C. Thomas, A. T. Hatke, P. Krogstrup, M. J. Manfra, K. Flensberg, and C. M. Marcus, Scaling of Majorana Zero-Bias Conductance Peaks, Phys. Rev. Lett. **119**, 136803 (2017).

[18] J. Chen, P. Yu, J. Stenger, M. Hocevar, D. Car, S. R. Plissard, E. P. A. M. Bakkers, T. D. Stanescu, and S. M. Frolov, Experimental phase diagram of zero-bias conductance peaks in superconductor/semiconductor nanowire devices, Sci. Adv. **3**, e1701476 (2017).

[19] D. Sherman, J. S. Yodh, S. M. Albrecht, J. Nygård, P. Krogstrup, and C. M. Marcus, Normal, superconducting and topological regimes of hybrid double quantum dots, Nat. Nanotechnol. **12**, 212 (2017).

[20] H. Zhang, C.-X. Liu, S. Gazibegovic, D. Xu, J. A. Logan, G. Wang, N. van Loo, J. D. S. Bommer, M. W. A. de Moor, D. Car, R. L. M. Op het Veld, P. J. van Veldhoven, S. Koelling, M. A. Verheijen, M. Pendharkar, D. J. Pennachio, B. Shojaei, J. S. Lee, C. J. Palmstrom, E. P. A. M. Bakkers, S. D. Sarma, and L. P. Kouwenhoven, Quantized Majorana conductance, Nature (London) **556**, 74 (2018).

[21] M.-T. Deng, S. Vaitiekėnas, E. Prada, P. San-Jose, J. Nygård, P. Krogstrup, R. Aguado, and C. M. Marcus, Nonlocality of Majorana modes in hybrid nanowires, Phys. Rev. B **98**, 085125 (2018).

[22] D. M. T. van Zanten, D. Sabonis, J. Suter, J. I. Väyrynen, T. Karzig, D. I. Pikulin, E. C. T. O'Farrell, D. Razmadze, K. D. Petersson, P. Krogstrup, and C. M. Marcus, Photon-assisted tunneling of zero modes in a Majorana wire, Nat. Phys. **16**, 663 (2020).

[23] S. Nadj-Perge, I. K. Drozdov, J. Li, H. Chen, S. Jeon, J. Seo, A. H. MacDonald, B. A. Bernevig, and A. Yazdani, Observation of Majorana fermions in ferromagnetic atomic chains on a superconductor, Science **346**, 602 (2014).

[24] Q. L. He, L. Pan, A. L. Stern, E. C. Burks, X. Che, G. Yin, J. Wang, B. Lian, Q. Zhou, E. S. Choi, K. Murata, X. Kou, Z. Chen, T. Nie, Q. Shao, Y. Fan, S.-C. Zhang, K. Liu, J. Xia, and K. L. Wang, Chiral Majorana fermion modes in a quantum anomalous Hall insulator–superconductor structure, Science **357**, 294 (2017).

[25] M. Kayyalha, D. Xiao, R. Zhang, J. Shin, J. Jiang, F. Wang, Y.-F. Zhao, R. Xiao, L. Zhang, K. M. Fijalkowski, P. Mandal, M. Winnerlein, C. Gould, Q. Li, L. W. Molenkamp, M. H. W. Chan, N. Samarth, and C.-Z. Chang, Absence of evidence for chiral Majorana modes in quantum anomalous Hall-superconductor devices, Science **367**, 64 (2020).

[26] A. Fornieri, A. M. Whiticar, F. Setiawan, E. Portolès, A. C. C. Drachmann, A. Keselman, S. Gronin, C. Thomas, T. Wang, R. Kallaher, G. C. Gardner, E. Berg, M. J. Manfra, A. Stern, C. M. Marcus, and F. Nichele, Evidence of topological superconductivity in planar Josephson junctions, Nature (London) **569**, 89 (2019).

[27] M.-X. Wang, C. Liu, J.-P. Xu, F. Yang, L. Miao, M.-Y. Yao, C. L. Gao, C. Shen, X. Ma, X. Chen, Z.-A. Xu, Y. Liu, S.-C. Zhang, D. Qian, J.-F. Jia, and Q.-K. Xue, The Coexistence of Superconductivity and Topological Order in the Bi_2Se_3 Thin Films, Science **336**, 52 (2012).

[28] G. C. Ménard, A. Mesaros, C. Brun, F. Debontridder, D. Roditchev, P. Simon, and T. Cren, Isolated pairs of Majorana zero modes in a disordered superconducting lead monolayer, Nat. Commun. **10**, 2587 (2019).

[29] T. Machida, Y. Sun, S. Pyon, S. Takeda, Y. Kohsaka, T. Hanaguri, T. Sasagawa, and T. Tamegai, Zero-energy vortex bound state in the superconducting topological surface state of Fe(Se,Te), Nat. Mater. **18**, 811 (2019).

[30] D. Wang, L. Kong, P. Fan, H. Chen, S. Zhu, W. Liu, L. Cao, Y. Sun, S. Du, J. Schneeloch, R. Zhong, G. Gu, L. Fu, H. Ding, and H.-J. Gao, Evidence for Majorana bound states in an iron-based superconductor, Science **362**, 333 (2018).

[31] M. Leijnse and K. Flensberg, Introduction to topological superconductivity and Majorana fermions, Semicond. Sci. Technol. **27**, 124003 (2012).

[32] J. Alicea, New directions in the pursuit of Majorana fermions in solid state systems, Rep. Prog. Phys. **75**, 076501 (2012).

[33] C. Beenakker, Search for Majorana Fermions in Superconductors, Annu. Rev. Condens. Matter Phys. **4**, 113 (2013).

[34] T. D. Stanescu and S. Tewari, Majorana fermions in semiconductor nanowires: fundamentals, modeling, and experiment, J. Phys.: Condens. Matter **25**, 233201 (2013).

[35] S. R. Elliott and M. Franz, Colloquium: Majorana fermions in nuclear, particle, and solid-state physics, Rev. Mod. Phys. **87**, 137 (2015).

[36] S. D. Sarma, M. Freedman, and C. Nayak, Majorana zero modes and topological quantum computation, npj Quantum Inf. **1**, 15001 (2015).

[37] M. Sato and S. Fujimoto, Majorana fermions and topology in superconductors, J. Phys. Soc. Jpn. **85**, 072001 (2016).

[38] V. Lahtinen and J. K. Pachos, A Short Introduction to Topological Quantum Computation, Sci. Post. Phys. **3**, 021 (2017).

[39] R. Aguado, Majorana quasiparticles in condensed matter, Riv. Nuovo Cimento **40**, 523 (2017).

[40] J. C. Y. Teo and C. L. Kane, Topological defects and gapless modes in insulators and superconductors, Phys. Rev. B **82**, 115120 (2010).

[41] K. Shiozaki and M. Sato, Topology of crystalline insulators and superconductors, Phys. Rev. B **90**, 165114 (2014).

[42] M. Cheng, R. M. Lutchyn, V. Galitski, and S. Das Sarma, Splitting of Majorana-Fermion Modes due to Intervortex Tunneling in a $p_x + ip_y$ Superconductor, Phys. Rev. Lett. **103**, 107001 (2009).

[43] T. Mizushima and K. Machida, Splitting and oscillation of Majorana zero modes in the *p*-wave BCS-BEC evolution with plural vortices, Phys. Rev. A **82**, 023624 (2010).

[44] M. Matsumoto and R. Heeb, Vortex charging effect in a chiral $p_x \pm i p_y$-wave superconductor, Phys. Rev. B **65**, 014504 (2001).

[45] M. Takigawa, M. Ichioka, K. Machida, and M. Sigrist, Vortex structure in chiral *p*-wave superconductors, Phys. Rev. B **65**, 014508 (2001).

[46] S. Tewari, S. Das Sarma, C. Nayak, C. Zhang, and P. Zoller, Quantum Computation using Vortices and Majorana Zero Modes of a $p_x + i p_y$ Superfluid of Fermionic Cold Atoms, Phys. Rev. Lett. **98**, 010506 (2007).

[47] T. Mizushima, M. Ichioka, and K. Machida, Role of the Majorana Fermion and the Edge Mode in Chiral Superfluidity near a *p*-Wave Feshbach Resonance, Phys. Rev. Lett. **101**, 150409 (2008).

[48] Y. E. Kraus, A. Auerbach, H. A. Fertig, and S. H. Simon, Testing for Majorana Zero Modes in a $p_x + i p_y$ Superconductor at High Temperature by Tunneling Spectroscopy, Phys. Rev. Lett. **101**, 267002 (2008).

[49] Y. E. Kraus, A. Auerbach, H. A. Fertig, and S. H. Simon, Majorana fermions of a two-dimensional $p_x + i p_y$ superconductor, Phys. Rev. B **79**, 134515 (2009).

[50] T. Mizushima and K. Machida, Vortex structures and zero-energy states in the BCS-to-BEC evolution of *p*-wave resonant Fermi gases, Phys. Rev. A **81**, 053605 (2010).

[51] C. Caroli, P. De Gennes, and J. Matricon, Bound Fermion states on a vortex line in a type II superconductor, Phys. Lett. **9**, 307 (1964).

[52] C. S. Amorim, K. Ebihara, A. Yamakage, Y. Tanaka, and M. Sato, Majorana braiding dynamics in nanowires, Phys. Rev. B **91**, 174305 (2015).

[53] M. Sekania, S. Plugge, M. Greiter, R. Thomale, and P. Schmitteckert, Braiding errors in interacting Majorana quantum wires, Phys. Rev. B **96**, 094307 (2017).

[54] B. Bauer, T. Karzig, R. V. Mishmash, A. E. Antipov, and J. Alicea, Dynamics of Majorana-based qubits operated with an array of tunable gates, Sci. Post. Phys. **5**, 4 (2018).

[55] A. Wieckowski, M. Mierzejewski, and M. Kupczyński, Majorana phase gate based on the geometric phase, Phys. Rev. B **101**, 014504 (2020).

[56] W. Chen, J. Wang, Y. Wu, J. Liu, and X. C. Xie, Non-Abelian statistics of Majorana zero modes in the presence of an Andreev bound state, arXiv:2005.00735.

[57] T. Karzig, F. Pientka, G. Refael, and F. von Oppen, Shortcuts to non-Abelian braiding, Phys. Rev. B **91**, 201102(R) (2015).

[58] T. Karzig, G. Refael, and F. von Oppen, Boosting Majorana Zero Modes, Phys. Rev. X **3**, 041017 (2013).

[59] C. Knapp, M. Zaletel, D. E. Liu, M. Cheng, P. Bonderson, and C. Nayak, The Nature and Correction of Diabatic Errors in Anyon Braiding, Phys. Rev. X **6**, 041003 (2016).

[60] C. Tutschku, R. W. Reinthaler, C. Lei, A. H. MacDonald, and E. M. Hankiewicz, Majorana-based quantum computing in nanowire devices, Phys. Rev. B **102**, 125407 (2020).

[61] S. Fujimoto, Topological order and non-Abelian statistics in noncentrosymmetric *s*-wave superconductors, Phys. Rev. B **77**, 220501(R) (2008).

[62] M. Sato, Y. Takahashi, and S. Fujimoto, Non-Abelian Topological Order in *s*-Wave Superfluids of Ultracold Fermionic Atoms, Phys. Rev. Lett. **103**, 020401 (2009).

[63] M. Sato, Y. Takahashi, and S. Fujimoto, Non-Abelian topological orders and Majorana fermions in spin-singlet superconductors, Phys. Rev. B **82**, 134521 (2010).

[64] L. Fu and C. L. Kane, Superconducting Proximity Effect and Majorana Fermions at the Surface of a Topological Insulator, Phys. Rev. Lett. **100**, 096407 (2008).

[65] M. Cheng, V. Galitski, and S. Das Sarma, Nonadiabatic effects in the braiding of non-Abelian anyons in topological superconductors, Phys. Rev. B **84**, 104529 (2011).

[66] M. S. Scheurer and A. Shnirman, Nonadiabatic processes in Majorana qubit systems, Phys. Rev. B **88**, 064515 (2013).

[67] H. Tal-Ezer and R. Kosloff, An accurate and efficient scheme for propagating the time dependent Schrödinger equation, J. Chem. Phys. **81**, 3967 (1984).

[68] O. V. Astafiev, L. B. Ioffe, S. Kafanov, Y. A. Pashkin, K. Y. Arutyunov, D. Shahar, O. Cohen, and J. S. Tsai, Coherent quantum phase slip, Nature (London) **484**, 355 (2012).

[69] K. Masuda, S. Moriyama, Y. Morita, K. Komatsu, T. Takagi, T. Hashimoto, N. Miki, T. Tanabe, and H. Maki, Thermal and quantum phase slips in niobium-nitride nanowires based on suspended carbon nanotubes, Appl. Phys. Lett. **108**, 222601 (2016).

[70] S. Vijay, T. H. Hsieh, and L. Fu, Majorana Fermion Surface Code for Universal Quantum Computation, Phys. Rev. X **5**, 041038 (2015).

[71] S. Vijay and L. Fu, Physical implementation of a Majorana fermion surface code for fault-tolerant quantum computation, Phys. Scr. **T168**, 014002 (2016).

[72] See Supplemental Material at http://link.aps.org/supplemental/10.1103/PhysRevB.103.054504 for a movie of the numerical simulation of braiding dynamics in the two-vortex system and a movie of the numerical simulation of braiding dynamics in the four-vortex system.

[73] T. Hanaguri, S. Niitaka, K. Kuroki, and H. Takagi, Unconventional s-Wave Superconductivity in Fe(Se,Te), Science **328**, 474 (2010).

[74] S. Rinott, K. B. Chashka, A. Ribak, E. D. L. Rienks, A. Taleb-Ibrahimi, P. Le Fevre, F. Bertran, M. Randeria, and A. Kanigel, Tuning across the BCS-BEC crossover in the multiband superconductor Fe$_{1+y}$Se$_x$Te$_{1-x}$: An angle-resolved photoemission study, Sci. Adv. **3**, e1602372 (2017).

[75] M. Sato and S. Fujimoto, Existence of Majorana Fermions and Topological Order in Nodal Superconductors with Spin-Orbit Interactions in External Magnetic Fields, Phys. Rev. Lett. **105**, 217001 (2010).

[76] J. R. Kirtley, C. C. Tsuei, and K. A. Moler, Temperature Dependence of the Half-Integer Magnetic Flux Quantum, Science **285**, 1373 (1999).

[77] C. C. Tsuei, J. R. Kirtley, C. C. Chi, Yu-Jahnes, A. Gupta, T. Shaw, J. Z. Sun, and M. B. Ketchen, Pairing Symmetry and Flux Quantization in a Tricrystal Superconducting Ring of YBa$_2$Cu$_3$O$_{7-\delta}$, Phys. Rev. Lett. **73**, 593 (1994).

[78] J. R. Kirtley, C. C. Tsuei, M. Rupp, J. Z. Sun, L. S. Yu-Jahnes, A. Gupta, M. B. Ketchen, K. A. Moler, and M. Bhushan, Direct Imaging of Integer and Half-Integer Josephson Vortices in High-T_c Grain Boundaries, Phys. Rev. Lett. **76**, 1336 (1996).

[79] H.-H. Sun, K.-W. Zhang, L.-H. Hu, C. Li, G.-Y. Wang, H.-Y. Ma, Z.-A. Xu, C.-L. Gao, D.-D. Guan, Y.-Y. Li, C. Liu, D. Qian, Y. Zhou, L. Fu, S.-C. Li, F.-C. Zhang, and J.-F. Jia, Majorana Zero Mode Detected with Spin Selective Andreev Reflection in

the Vortex of a Topological Superconductor, Phys. Rev. Lett. **116**, 257003 (2016).

[80] B. H. November, J. D. Sau, J. R. Williams, and J. E. Hoffman, Scheme for Majorana manipulation using magnetic force microscopy, arXiv:1905.09792.

[81] H. S. Røising, R. Ilan, T. Meng, S. H. Simon, and F. Flicker, Finite temperature effects on Majorana bound states in chiral *p*-wave superconductors, Sci. Post. Phys. **6**, 55 (2019).

[82] M. Cheng, R. M. Lutchyn, and S. Das Sarma, Topological protection of Majorana qubits, Phys. Rev. B **85**, 165124 (2012).

[83] M. Sato, A. Yamakage, and T. Mizushima, Mirror Majorana zero modes in spinful superconductors/superfluids Non-Abelian anyons in integer quantum vortices, Phys. E (Amsterdam) **55**, 20 (2014).

[84] X.-J. Liu, C. L. M. Wong, and K. T. Law, Non-Abelian Majorana Doublets in Time-Reversal-Invariant Topological Superconductors, Phys. Rev. X **4**, 021018 (2014).

[85] A. Haim and Y. Oreg, Time-reversal-invariant topological superconductivity in one and two dimensions, Phys. Rep. **825**, 1 (2019).

[86] K. Wölms, A. Stern, and K. Flensberg, Local Adiabatic Mixing of Kramers Pairs of Majorana Bound States, Phys. Rev. Lett. **113**, 246401 (2014).

[87] P. Gao, Y.-P. He, and X.-J. Liu, Symmetry-protected non-Abelian braiding of Majorana Kramers pairs, Phys. Rev. B **94**, 224509 (2016).

[88] Y. Lin and A. J. Leggett, Effect of particle number conservation on the berry phase resulting from transport of a bound quasiparticle around a superfluid vortex, arXiv:1708.02578.

[89] Y. Lin and A. J. Leggett, Towards a particle-number conserving theory of majorana zero modes in p+ ip superfluids, arXiv:1803.08003.

[90] D. J. J. Marchand and M. Franz, Lattice model for the surface states of a topological insulator with applications to magnetic and exciton instabilities, Phys. Rev. B **86**, 155146 (2012).

[91] T. Liu and M. Franz, Electronic structure of topological superconductors in the presence of a vortex lattice, Phys. Rev. B **92**, 134519 (2015).

[92] M. Cheng, R. M. Lutchyn, V. Galitski, and S. Das Sarma, Tunneling of anyonic Majorana excitations in topological superconductors, Phys. Rev. B **82**, 094504 (2010).

[93] E. J. Weinberg, Index calculations for the fermion-vortex system, Phys. Rev. D **24**, 2669 (1981).

[94] T. Fukui and T. Fujiwara, Topological stability of Majorana zero modes in superconductor–topological insulator systems, J. Phys. Soc. Jpn. **79**, 033701 (2010).

[95] P. Zhang, K. Yaji, T. Hashimoto, Y. Ota, T. Kondo, K. Okazaki, Z. Wang, J. Wen, G. D. Gu, H. Ding, and S. Shin, Observation of topological superconductivity on the surface of an iron-based superconductor, Science **360**, 182 (2018).